AN EFFICIENT WORKFLOW TO ACCURATELY COMPUTE GROUNDWATER RECHARGE FOR THE STUDY OF RAINFALL-TRIGGERED DEEP-SEATED LANDSLIDES, APPLICATION TO THE SÉCHILIENNE UNSTABLE SLOPE (WESTERN ALPS)

Vallet A.[1], Bertrand C.[1], Fabbri O.[1], Mudry J.[1]

[1] UMR6249 Chrono-Environnement - Université de Franche-Comté - 16 route de Gray - F-25030 Besançon cedex – France

Abstract

Pore water pressure build-up by recharge of underground hydrosystems is one of the main triggering factors of deep-seated landslides. In most deep-seated landslides, pore water pressure data are not available since piezometers, if any, have a very short lifespan because of slope movements. As a consequence, indirect parameters, such as the calculated recharge, are the only data which enable to understand landslide hydrodynamic behaviour. However, in landslide studies, methods and recharge-area parameters used to determine the groundwater recharge are rarely detailed. In this study, the groundwater recharge is estimated with a soil-water balance based on characterization of evapotranspiration and parameters characterising the recharge area (soil-available water-capacity, runoff and vegetation coefficient). A workflow to compute daily groundwater recharge is developed. This workflow requires the records of precipitation, air temperature, relative humidity, solar radiation and wind speed within or close to the landslide area. The determination of the parameters of the recharge area is based on a spatial analysis requiring field observations and spatial datasets (digital elevation models, aerial photographs and geological maps). This study demonstrates that the performance of the correlation with landslide displacement velocity data is significantly improved using the recharge estimated with the proposed workflow. The coefficient of determination obtained with the recharge estimated with the proposed workflow is 78% higher on average than that obtained with precipitation, and is 38% higher on average than that obtained with recharge computed with a commonly used simplification in landslide studies (recharge = precipitation minus non-calibrated evapotranspiration method).

1. Introduction

Pore water pressure build-up by recharge of aquifers is one of the main triggering factors of destabilisation of deep-seated landslides (Noverraz et al., 1998; Van Asch et al., 1999; Guglielmi et al., 2005; Bogaard et al., 2007; Bonzanigo et al., 2007). In most deep-seated landslides, pore water pressure data are not available since piezometers, if any, have a very short lifespan because of slope movements. In addition, landslides show heterogeneous, anisotropic and discontinuous properties (Cappa et al., 2004; Binet et al., 2007a) and local measurements are rarely representative of the overall behaviour of the landslide aquifers. In the absence of piezometric measurements, the groundwater recharge is used as the most relevant parameter to characterize the pore water pressure of the landslide aquifers. Groundwater recharge (hereafter recharge), also referred to as deep percolation, is the part of the precipitation which recharges the saturated zones (aquifers).

Landslide studies involve a wide range of specialities (sub-surface geophysics, structural geology, modelling, geotechnics, and geomechanics). Scientists or engineers in charge of landslides may not have the required hydrology knowledge to accurately estimate the recharge. In most cases, deep-seated landslide studies devoted to characterise the rainfall-destabilisation relationships do not take into account recharge with enough accuracy. In particular, some studies estimate the recharge without calibration of the evapotranspiration estimation methods and without soil-water balance (Canuti et al., 1985; Alfonsi, 1997; Hong et al., 2005; Binet et al., 2007b; Durville et al., 2009; Pisani et al., 2010; Prokešová et al., 2013). Lastly, several studies use precipitation data instead of the recharge (Rochet et al., 1994; Zêzere et al., 2005; Meric et al., 2006; Helmstetter and Garambois, 2010; Belle et al., 2013). These approaches can over-estimate the groundwater recharge and can thus bias the characterisation of the relationship between rainfall and destabilisation. A more accurate estimation of the groundwater recharge signal can improve the accuracy of these studies. So far, no computation workflow has been proposed to estimate simply and accurately the recharge in the context of landslide studies.

Patwardhan et al. (1990) showed that the soil-water balance method is an accurate way to estimate groundwater recharge. Recharge computation with a soil-water balance depends mainly on the surface runoff, the soil-available water-capacity (SAWC) and the specific vegetation (so-called crop) evapotranspiration (ET_c, also referred to as potential evapotranspiration), itself being deduced from reference vegetation evapotranspiration (ET_0) with a vegetation coefficient (K_c). The Penman-Monteith method (Eq. (A6) in appendix A)), hereafter referred to as the ET_0 standard equation or FAO-56 PM, developed in the paper FAO-56 (Food and Agriculture Organization of the United Nations) is considered by the scientific community as a global standard method to estimate ET_0 worldwide (Jensen et al., 1990; Allen et al., 1998). This method requires the knowledge of the air relative humidity, the air temperature, the wind speed and the solar radiation. However, most weather stations in landslide areas record only air temperature and rainfall. Unlike the FAO-56 PM method, methods based only on air temperature and solar radiation (R_s) allow a simpler expression of ET_0 (Tabari et al., 2013). Besides, R_s can also be estimated only from air temperature (Almorox, 2011), thus allowing ET_0 to be obtained only from air temperature records. These reduced-set methods are developed under specific site conditions and must be calibrated in order to improve accuracy (Allen et al., 1994; Shahidian et al., 2012).

The objective of this study is to develop a parsimonious, yet robust, guideline workflow to calculate time series of groundwater recharge at the scale of the recharge area, time series that can subsequently be used as a deterministic variable in landslide studies. To maximize the accessibility to diverse user groups, we strive to develop an efficient method, balancing

technical accuracy with operational simplicity. The proposed workflow is applied on the deep-seated Séchilienne landslide. To test its utility, a correlation analysis is used to evaluate whether the calculated groundwater recharge is more strongly correlated with measured land mass displacement velocities than with precipitation or with recharge estimated with a common simplification in landslide studies (recharge = precipitation minus non-calibrated ET_0; Canuti et al., 1985; Binet et al., 2007; Pisani et al., 2010; Prokešová et al., 2013). The significance of the correlations is assessed with bootstrap tests. The proposed study aims at showing that an accurate estimation of the recharge can significantly improve the results of rainfall-displacement studies.

2. Method

2.1. General workflow

In the case of deep-seated landslides triggered by deep water-saturated zones, the impact of a multi-day cumulative rainfall is far more significant than rainfall duration or intensity (Van Asch et al., 1999; Guzzetti et al., 2008). For these reasons, the workflow is developed to compute daily groundwater recharge. Similarly, this study is based on displacement recorded at a daily time-step. For the sake of simplicity, the daily displacement, equivalent to a velocity measurement in mm/day, is hereafter referred to as displacement. The groundwater recharge is estimated with a soil-water balance based on characterization of ET_0 and parameters characterising the recharge area (SAWC, runoff and K_c). The computation workflow (Fig. 1), hereafter referred to as LRIW (Landslide Recharge Input Workflow), includes four steps.

The estimation of the ET_0 requires the records of air temperature within the landslide area and relative humidity, solar radiation and wind speed within or close to the landslide area. In the case of a landslide-located weather station recording only the temperature, the first step (detailed in section 2.2) consists of a regional calibration of ET_0 and R_S reduced-set equations (equations detailed in appendix A). The calibrated methods then allow to estimate evapotranspiration based only on temperature records. In the case of a landslide weather station recording the full set of parameters, the first step can be skipped and the FAO-56 PM method can then be used to estimate ET_0. The second step (detailed in section 2.3) consists in estimating the recharge-area parameters (surface runoff, SAWC and K_c) using a GIS (Geographic Information Systems) composite method requiring field observations and spatial datasets (digital elevation models, aerial photographs and geological maps). The third step (detailed in section 2.4) uses a soil-water balance to estimate the recharge with the estimated ET_0 and the estimation of the recharge-area parameters. The fourth step (detailed in section 2.5) consists of a sensitivity analysis based on a recharge-displacement velocity correlation and is performed in order to refine the estimations of SAWC and runoff coefficient.

2.2. Step 1: Regional calibration of ET_0 and R_S methods

ET_0 reduced-set and R_S temperature methods were initially developed for given regions or sites with their own climatic conditions and must be calibrated to take into account the weather conditions of the study site. Details about calibration can be found in the literature (Allen et al., 1994; Itenfisu et al., 2003; Lu et al., 2005; Alkaeed et al., 2006; Alexandris et al., 2008; Shahidian et al., 2012; Tabari et al., 2013).

The regional calibration method (Fig. 1– Step 1) is performed using the records of nearby weather stations (hereafter referred to as reference weather stations) having similar climatic conditions as the study site and recording the required meteorological parameters. The calibration of R_S and ET_0 methods are performed for each reference weather station (local

scale). The local adjustment coefficients of the reference stations are then averaged in order to define a regional calibration. The user has to maintain a balance between the number of selected reference stations and the necessity for these stations to be located in areas with climatic conditions similar to those of the study site. For sites with a sparse weather station network, one reference station can be sufficient for the calibration, provided that this station has the same weather conditions as those of the studied site.

The performance assessment of regional-scale calibrated methods is based on the comparison between observed measurements and calibrated estimates for R_s and between FAO-56 PM estimates and calibrated estimates for ET_0 for each reference weather station. Performance indicators are the coefficient of determination (R^2), the slope and the intercept from linear regression (independent variable: estimated parameter; dependant variable: reference parameter), and the root mean square error (RMSE).

2.2.1. Solar radiation methods

Bristow and Campbell (1984) and Hargreaves and Samani (1985) proposed methods to compute R_S based solely on the air temperature measurement (Eq. (A1) and Eq. (A2) in appendix A). Castellvi (2001) demonstrated that both methods show good results for daily frequencies. The coefficients of the Bristow-Campbell method have to be evaluated. The coefficients of the Hargreaves-Samani method have default values. However, Trajkovic (2007) showed that the regional calibration of the Hargreaves-Samani method is significantly improved by an adjustment of the coefficients rather than by a linear regression. Therefore, all the HS_{mod} R_s coefficients are adjusted. In this study, modified forms of the Bristow-Campbell method (Eq. (A3)) and Hargreaves-Samani method (Eq. (A4)) are used. For the R_S equations, the adjustment of the local calibration coefficients is non-linear. To adjust the calibration coefficients, a grid search iterative algorithm is used to maximise the R^2 value while minimizing the RMSE at each reference weather station.

2.2.2. Evapotranspiration methods

ET_0 is the evapotranspiration from a reference grass surface and is used as a standard from which ET_c is deduced as follows (Allen et al., 1998):

$$ET_c = ET_0 \times K_c \quad (1)$$

where K_c is the vegetation coefficient.

Several ET_0 methods using a reduced dataset in comparison to the FAO-56 PM method have been developed worldwide. Only a few methods are commonly used. This is the case with the five ET_0 methods selected for this study, which have shown good performance when using daily to weekly frequencies (Trajkovic, 2005; Yoder et al., 2005; Alexandris et al., 2008; Shahidian et al., 2012; Tabari et al., 2013). The five selected ET_0 methods, namely the methods of Hargreaves-Samani (1985), Makkink (1957), Turc (1961), Priestley and Taylor (1972), and the Penman-Monteith reduced-set method (Allen et al., 1998), require records of R_S and temperature (Eq. (A7) to Eq. (A12) in appendix A). As R_S can be estimated with a calibrated R_S temperature-based method, ET_0 can thus be obtained with temperature records only.

ET_0 is calculated using data collected at each reference weather stations (independent ET_0 estimates). These calculations follow FAO-56 PM method outlined in the FAO-56 document (Allen et al., 1998). These independent ET_0 estimates are then used as pseudo-standards for

the purpose of calibrating the regional-scale ET_0 methods. A linear regression is performed for each of the evapotranspiration methods and for each reference weather station (Eq. (2)). The slope *a* and the intercept *b* of the best-fit regression line are used as local calibration coefficients.

$$ET_{0\,FAO-56\,PM} = a\,ET_{0\,method} + b \tag{2}$$

where $ET_{0\ FAO\text{-}56\ PM}$ is the ET_0 estimated with the standard method and $ET_{0\ method}$ is the ET_0 obtained by any of the five methods tested in this study. The linear regression method has been widely used to calibrate ET_0 methods (Allen et al., 1994; Trajkovic, 2005; Shahidian et al., 2012).

2.3.Step 2: Estimation of the parameters of the recharge area

The estimation of the recharge with the soil-water balance (step 3 – section 2.4) requires the calculation, at the scale of the recharge area, of three parameters which are SAWC, runoff coefficient R_{coeff}, and K_c. These three parameters are controlled by one or several factors which are, in this study, the slope gradient, the geological nature of the substratum and the type of vegetation cover. Besides, at the scale of the recharge area, the controlling factors are commonly heterogeneous and thus the recharge-area parameters cannot be readily computed. For each of the controlling factors, the recharge area is divided into sub-areas (hereafter referred to as factor sub-areas) characterized by homogenous factor properties. Factor sub-areas can be either continuous or discontinuous, and their number and shape can differ, depending of the spatial distribution of the factors. Relevant factor sub-areas are in turn used to define parameter sub-areas. For a given parameter sub-area, the value of the parameter is estimated from either field measurements or from the literature. The parameter values at the scale of the recharge area are then calculated by taking into account the relative surface of the parameter sub-areas (Fig. 1 – Step 2). Lastly, if preferential infiltration structures (hereafter referred to as infiltration structures) such as sinkholes, cracks, reverse slope areas, bare ground or any topographical depression which can collect the surface runoff are present in the recharge area, the above-mentioned parameters have to be adjusted. For such areas, the SAWC and R_{coeff}, being very low, will be set at zero in the calculations. Similarly, for such areas, ET_0 is negligible and therefore the surface of these areas is disregarded for the K_c computation. The parameter values are afterwards refined by a sensitivity analysis (step 4-section 2.5) in order to find the optimal set of recharge-area parameters.

The K_c parameter takes into account four key characteristics (vegetation height, albedo, canopy resistance and evaporation from soil) that distinguish the vegetation type of a given sub-area from the reference grass used to estimate ET_0 (Allen et al., 1998). The K_c sub-areas are defined according to the type of vegetation (e.g., meadow, forest…) obtained from aerial photographs. The dominant vegetation species assigned to each vegetation type can be obtained from literature (e.g., forest agency data) or from field observations. Since the K_c parameter depends on the stage of development of the vegetation, it varies from a minimum value during winter to a maximum value during summer. The minimum and maximum K_c values are estimated from the literature and are assigned respectively to the 4th of February (middle of winter) and the 6th of August (middle of summer) of each year. A daily linear interpolation is performed for K_c between these two dates (Verstraeten et al., 2005).

The SAWC parameter refers to the difference between a maximum water content above which all free water is drained through gravity (field capacity) and a minimum moisture content below which plant roots cannot extract any water (permanent wilting point). The

SAWC is mainly affected by soil texture and thickness, both depending primarily on the geological substratum and the vegetation. The SAWC sub-areas are defined according to the type of vegetation (obtained from aerial photographs) and to the geological substratum (obtained from geological maps). SAWC values can be either calculated with pedotransfer functions (Bruand et al., 2004; Pachepsky and Rawls, 2004) from soil properties (type of horizon, texture and bulk density) and thickness or obtained directly from the literature. Soil properties and thickness can be obtained from the literature (e.g., pedological maps) or from morphological description or laboratory measurements of auger hole cores.

The method used to estimate the surface runoff is similar to the commonly used 'runoff rational method'. The R_{coeff} parameter depends mainly on topography and vegetation. The R_{coeff} sub-areas are defined according to the vegetation (obtained from aerial photographs). An average slope gradient obtained from the DEM is assigned to each vegetation sub-area. The R_{coeff} values can then be calculated from vegetation cover and slope gradient through the use of charts such as the Sautier chart (Musy and Higy, 2011).

Infiltration structures are first located through examination of aerial photographs (lineaments analysis) and geological maps, and are then inspected in the field.

2.4.Step 3: Recharge computation with soil-water balance

The soil-water balance workflow used to estimate the recharge at a daily frequency is detailed in Fig. 2. All terms required for the soil-water balance estimation are expressed in water amount (millimetres), except for R_{coeff} expressed in %. The soil-water balance is based on ET_c, SAWC, K_c and R_{coeff}. The precipitation (P) is the amount of liquid (rain) or solid (snow) water which falls on the recharge area. The precipitation will be taken here as the sum of snow melt and rainfall. A part of this water amount is intercepted by the vegetative canopy (interception; Fig. 2A). The remainder of precipitation reaches the ground surface and forms (i) the runoff (Rf), which is the water joining the surface drainage network and (ii) the infiltration (I) into the soil layer which supplies the SAWC. The remaining part of the precipitation not uptaken by evapotranspiration and runoff and not stored in the SAWC is called the recharge (R). It corresponds to deep percolation and is the component of the precipitation which recharges the saturated zone (Fig. 2A).

The ET_c is a lumped parameter including potential transpiration, potential soil evaporation and canopy interception evaporation (Verstraeten et al., 2005). In the proposed computation diagram workflow (Fig. 2B) the interception component is therefore integrated in the ET_c component. The ET_c is the water evapotranspired without any other restrictions than the atmospheric demand (assuming unlimited soil water availability). However, field conditions do not always fulfil these requirements, particularly during low rainfall periods when water supplies are inadequate to support vegetation uptakes. The actual evapotranspiration (ET_a) corresponds to the actual amount of evapotranspired water.

Runoff takes place when the intensity of a precipitation event exceeds the soil infiltration capacity. The use of a daily measurement frequency for precipitation does not allow an accurate estimation of rainfall intensity. Instead, a R_{coeff} is applied only for days when precipitation is greater than the average. Such days are considered as high intensity rainfall days. The R_{coeff} is applied only to excess precipitation, after the demands of evapotranspiration and SAWC are met, i.e., when SAWC is fulfilled (Fig. 2B).

2.5. Step 4: Sensitivity analysis of the recharge-area parameters

In the landslide recharge area, recharge can be considered as spatially heterogeneous. Indeed, in fractured rocks, the groundwater flow is mainly driven by an anisotropic fracture network. The proportion of infiltrated water which flows toward the landslide aquifer can significantly differ between two zones of the recharge area. Nevertheless, the GIS composite method considers that any part of the recharge area has the same weight with respect to the groundwater which flows toward the landslide aquifer. This homogeneous recharge assumption can lead to biased estimations of the recharge-area parameters. On the other hand, uncertainties in the delimitation of the recharge area can also lead to biased estimations.

A sensitivity analysis evaluates the possible over-estimation or under-estimation of the set of recharge-area parameters. The infiltration-structure sub-areas are used as fitting factors (varying from 0 to 100% of the recharge area surface) to adjust the estimation of the set of recharge-area parameters. A variation of the infiltration structure percentage corresponds to a variation of the contribution weight of the infiltration structures to the recharge of the landslide aquifer. Consequently, a variation of the infiltration structure percentage does not affect the relative proportion of the other sub-area surfaces but only their contribution weights. The sensitivity analysis is based on the performance of a linear correlation between daily time series of recharge and displacement. The landslide displacement triggered by pore water pressure is therefore related to the hydrodynamic variations of the landslide aquifers. For this reason, the performance of the correlation between recharge and displacement informs whether the recharge-area parameters are satisfactorily estimated. The sensitivity analysis allows to determine the optimal set of recharge-area parameters which maximize the performance of the correlation.

2.6. Correlation between water input and displacement

2.6.1. Antecedent cumulative sum

The correlation between water input and displacement requires measurements of landslide displacements at the same temporal frequency (daily frequency in this study) as the measurements of water input (precipitation or recharge). The groundwater hydrodynamic processes in aquifers are non-linear. A former rainfall event displays less impact (though not negligible) than a recent one on the aquifer hydrodynamic fluctuations (Canuti et al., 1985; Crozier, 1986; Diodato et al., 2014). The daily precipitation/recharge time series cannot therefore be used without appropriate corrections. An antecedent cumulative sum of precipitation/recharge weighted by a factor α is applied as a moving window to the daily precipitation/recharge time series (Eq. (3)). The antecedent cumulative sum allows to approximate the daily triggering impact of the aquifer *ATI* on the landslide destabilisation. In order to take into account the groundwater transit time, a β time-lag factor is introduced. This factor can shift the moving window from the target date *t*.

$$ATI_t = \sum_{i=t+\beta}^{t+\beta+n} \frac{W_i}{1+\alpha\ (\mathrm{i} - (\mathrm{t}+\beta))} \quad (3)$$

where:

ATI_t Aquifer Triggering Impact at the date t (in mm)

β time shift of the moving window (in days)

i i^{th} day from the date t (i=t+β: start of the moving window and i= t+β +n: end of the moving window)

n length of the moving window of the cumulative period (in days)

W_i water input, i.e., precipitation or recharge at the i^{th} day (in mm)

α weighting factor

An iterative grid search algorithm is used to find the optimal set of parameters of the antecedent cumulative sum. The optimal set of parameters is the set that maximizes the correlation performance itself based on the R^2 indicator. The grid search algorithm investigates the following parameter ranges: n from 1 to 250 days (increment: 1 day), α from 0 to 0.5 (increment: 0.0001) and β from 1 to 10 days (increment: 1 day).

2.6.2. Significance of the water input-displacement correlation

The bootstrap method, which is an inference statistical resampling method, is used to estimate the confidence interval (CI) of estimated parameters and to perform statistical hypothesis tests (Chernick, 2008). The bootstrap method uses resampling with replacement and preserves the pair-wise relationship. However, for inter-dependent data (such as time series), the structure of the dataset has to be preserved during the resampling. The moving block bootstrap is a variant of the bootstrap method. It divides data into blocks for which the structure is kept (Cordeiro and Neves, 2006). The moving block bootstrap method is performed with a 90-day block size (season) and 50,000 iterations for each run.

To estimate the significance of the linear regression, the lower bound of the confidence interval (LBCI) of R^2 is used at the level of confidence of 95%. An LBCI value greater than 0 means that the relationship is significant. Particular to statistical hypothesis tests is the definition of the tested null hypothesis which is often a default position opposite to the aim of the test, i.e. by stating that "there is no relationship between the two considered quantities". The null hypothesis is assumed to be true until it is rejected by statistical evidence in favour of the alternative opposite hypothesis. The recharge estimated with the LRIW workflow is hereafter called R_{LRIW}. The recharge estimated by subtracting a non-calibrated ET_0 from precipitation is hereafter called R_{PMNE}, PMNE standing for Precipitation Minus Non-calibrated ET_0.

To estimate whether the R_{PMNE}/displacement correlation R^2 is significantly better than the precipitation/displacement correlation R^2 value, the Null Hypothesis 1 (NH1) is tested. The NH1 states that the R_{PMNE}/displacement correlation R^2 value is not significantly greater than the R^2 value obtained from precipitation. In other words, the NH1 statistic test is the difference between the R_{PMNE} R^2 value and the precipitation R^2 value, expected to be 0 if no difference. Similarly, the Null Hypothesis 2 (NH2) and the Null Hypothesis 3 (NH3) are tested. NH2 estimates whether the R_{LRIW}/displacement correlation R^2 is significantly better than the precipitation/displacement correlation R^2 value. NH3 estimates whether the

R_{LRIW}/displacement correlation R^2 is significantly better than the R_{PMNE}/displacement correlation R^2 value.

To estimate whether the best precipitation-R_{LRIW}/displacement correlation R^2 value computed from the sensitivity analysis is significantly better than the other R^2 values obtained, the Null Hypothesis 4 (NH4) is tested. The NH4 states that the best R^2 value is not significantly greater than the ones obtained with all the remaining combinations. In other words, the NH4 statistic test is the difference between the best R^2 value and the R^2 values obtained with the remaining combinations, expected to be 0 if no difference.

For all null hypotheses, the decision of rejection is made by determining how much of the bootstrap distribution (among 50,000 iterations) falls below zero by using the lower bound of the confidence interval (LBCI) at the level of confidence of 95%. An LBCI value greater than 0 allows to reject the null hypotheses.

3. Application to the Séchilienne landslide

3.1. Geological settings and rainfall triggering

The Séchilienne landslide is located in the French Alps on the right bank of the Romanche river, on the southern slope of the Mont-Sec Massif (Fig. 3). The climate is mountainous with a mean annual precipitation height of 1200 mm. The geological nature of the area is composed of vertical N-S foliated micaschists unconformably covered by Carboniferous to Liassic sedimentary deposits along the massif ridge line above the unstable zone. Quaternary glacio-fluvial deposits are also present. The Séchilienne landslide is limited eastwards by a N-S fault scarp and northwards by a major head scarp of several hundred meters wide and tens of meters high below the Mont Sec. The slope is cut by a dense network of two sets of near-vertical open fractures trending N110 to N120 and N70 (Le Roux et al., 2011).

The Séchilienne landslide is characterized by a deep progressive deformation controlled by the network of faults and fractures. A particularity of the Séchilienne landslide is the absence of a well-defined basal sliding surface. The landslide is affected by a deeply rooted (about 100-150 m) toppling movement of the N50-70° slabs to the valley (accumulation zone) coupled with the sagging of the upper slope (depletion zone) beneath the Mont Sec (Vengeon, 1998; Durville et al., 2009; Lebrouc et al., 2013). A very active moving zone is distinguishable from the unstable slope where high displacement velocities can be 10-time higher than the rest of the landslide.

The landslide shows a higher hydraulic conductivity than the underlying stable bedrock (Vengeon, 1998; Meric et al., 2005; Le Roux et al., 2011), thus leading to a landslide perched aquifer (Guglielmi et al., 2002). The recharge of the landslide perched aquifer is essentially local, enhanced by the trenches and the counterscarps which tend to limit the runoff and to facilitate groundwater infiltration in the landslide area. However, the hydrochemical analyses of Guglielmi et al. (2002) shows that the sedimentary deposits distributed above the landslide hold a perched aquifer which can recharge the landslide perched aquifer. The fractured metamorphic bedrock beneath the landslide contains a deep satured zone at the base of the slope and an overlying vadose zone. The groundwater flow of the entire massif is mainly controlled by the network of fractures with high flow velocities (up to a few kilometres per day; Mudry and Etievant, 2007). The hydromechanical study of Cappa et al. (2014) shows that the deep aquifer can also trigger the Séchilienne landslide destabilization as a result of stress transfer and frictional weakening. Thus, the Séchilienne landslide destabilisation is likely triggered by a two-layer hydrosystem: the landslide perched aquifer and the deep aquifer. The Séchilienne landslide behaviour is characterized by a good correlation between

precipitations and displacement velocities (Rochet et al., 1994; Alfonsi, 1997; Durville et al., 2009; Chanut et al., 2013).The seasonal variations of the daily displacements are clearly linked to the seasonal variations of the recharge (high displacements during high flow periods and low displacements during low flow periods).

3.2.Method implementation

The recharge computation uses the daily rainfall recorded at the weather station located at Mont-Sec, a few hundred meters above the top of the landslide (Table 1 and Fig. 3). This station is equipped with rain and snow gauges and a temperature sensor. However, the temperature measurements at the Mont-Sec station are considered unreliable because of a non-standard setting of the temperature sensor and numerous missing data. Consequently, the temperature at the Mont-Sec station has to be estimated in order to estimate the evapotranspiration at the landslide site (see details about the computation in appendix B).

Since the Mont-Sec station does not record the full set of parameters (relative humidity, temperature, wind speed and solar radiation), a regional calibration of ET_0 and R_S reduced-set methods is required. Three weather stations located at less than 60 kilometres from the studied site are used as reference weather stations: Grenoble-Saint-Geoirs, Saint-Jean-Saint-Nicolas and Saint-Michel-Maur (Table 1 and Fig. 3). The Saint-Michel-Maur weather station does not measure R_S, which is estimated with the Angström formula (Eq. (A5) in Appendix A) using sunshine duration data recorded at the station. The Angström formula empirical default coefficients are tuned with the two others weather stations ($a_S = 0.232$ and $b_S = 0.574$).

The delimitation of the recharge area of the two-layer hydrosystem (Fig. 3) of the Séchilienne landslide is based on the geological and hydrochemical studies of Vengeon (1998), Guglielmi et al. (2002) and Mudry and Etievant (2007). The recharge area is delimited by the spatial extent of the sedimentary cover of which the hosting perched aquifer recharges the two-layer hydrosystem. Groundwater flow of the entire Mont-Sec massif is controlled by faults and fractures. The N20 fault bordering the sedimentary cover to the east as well as the N-S fault zone bordering the landslide to the east are structures which delimitate the recharge area. The scarcity of information does not allow to accurately define the actual extent of the recharge area. The sensitivity analysis mentioned in Section 2.5 allows to compensate for the possible biases introduced by this uncertainty. The following spatial datasets are used for the estimation of the parameters of the recharge area. The aerial photographs (0.5 m resolution) and a DEM of 25 m resolution are provided by the “Institut National de l’Information Géographique et Forestière” (IGN) and geological maps are provided by the French Geological Survey (BRGM).

The Séchilienne landslide is permanently monitored by a dense network of displacement stations managed by the CEREMA Lyon (Duranthon et al., 2003). In this study, one infra-red station (1101) and three extensometer stations (A16, A13 and G5) are used. Stations 1101, A13 and A16 are representative of the most active zone (median displacement of 2.5, 1.75 and 2.98 mm/day, respectively), while G5 is located on a much less active zone (median displacement of 0.05 mm/day, Fig. 3 and Table 2).

The sensitivity analysis is performed on the A16 extensometer on the period from 01 May 1994 to 01 January 2012, period during which both A16 extensometer and recharge datasets are available. The performance test of the LRIW workflow against precipitation and R_{PMNE} is performed on the four displacements stations on the period from 01 January 2001 to 01 January 2012, period during which the four stations and recharge datasets are available. The R_{PMNE} is estimated with the non-calibrated Turc equation (Eq. (A8)) which is the most

appropriate ET_0 reduced-set equation for the Séchilienne site. Indeed, the Turc equation was developed initially for the climate of France. The Turc equation requires the estimation of R_s which is performed with the non-calibrated Hargreave-Samani equation (Eq. (A2)).

3.3. Displacement data detrending

The long-term displacement monitoring shows that displacement rate and amplitude exponentially increased with time as illustrated by the records of extensometer A16 (Fig. 4A). The rainfall data series does not show any trend over the year, meaning that the displacement trend is independent of the recharge amount. Consequently, on the Séchilienne landslide, for the same amount of rainfall, the displacement rate and magnitude responses increase steadily with time. The observed trend is the consequence of a progressive weakening of the landslide due to long-term repetitive stresses. The accumulating deformation can be assimilated to long-term creep (Brückl, 2001; Bonzanigo et al., 2007) and can be explained by a decrease of the slope shear strength (Rutqvist and Stephansson, 2003). As shown by the detrended displacement, the Séchilienne landslide is constantly moving and shows large daily to seasonal variations which seem to be the landslide response to the precipitation trigger. Consequently, the precipitation-displacement correlation is performed on the detrended displacement.

The exponential trend is removed with the statistical multiplicative method ($y_t = T_t S_t I_t$) where the time series (y_t) is composed of three components (Madsen, 2007; Cowpertwait and Metcalfe, 2009; Aragon, 2011): trend (T_t), seasonal (S_t) and irregular (I_t). In this study, the irregular and seasonal components are both assumed to be linked to the rainfall triggering factor ($y_t = T_t D_t \ with \ D_t = S_t I_t$). The trend is determined by curve fitting of a fourth-order polynomial (parametric detrending). The result is a detrended unitless time series (D_t) with both variance and mean trend removed. The time series decomposition process is illustrated with the A16 extensometer in Fig. 4.

4. Results of the recharge estimation with the LRIW method

4.1. Calibration of R_S and ET_0 methods

The two calibrated R_S methods show good results with respect to R_S measured at the reference weather stations. The BC_{mod} R_s method is selected as it shows a better performance (R^2 = 0.864; RMSE = 1.567) than the HS_{mod} R_s method (R^2 = 0.847; RMSE = 1.625). The equation (4) presents the calibrated BC R_s method with all the calibrated coefficients.

$$BC_{mod}\ R_s = 0.669\ Ra\left[1 - \exp\left(-0.010\ (\alpha \Delta T)^{2.053}\right)\right] + 1.733 \quad (4)$$

The cloud cover adjustment factor α is either equal to 0.79 (cloud impact) or to 1. All the equation terms are described in the Appendix A. The BC_{mod} R_s calibrated method is then used to compute R_s input data of the five ET_0 reduced-set methods.

Overall, all of the ET_0 methods tested show good results for regional calibration and are all suitable for the Séchilienne site (Table 3). Among the ET_0 methods tested, the PM_{red} ET_0 method shows the best performance (R^2 = 0.932; RMSE=0.505) and requires only a low regional adjustment (a = 0.994 and b = 0.013). Therefore, the PM_{red} ET_0 method is selected to compute ET_0 for the Séchilienne site (hereafter referred to as ET_0 Séch). Figure 5 displays the estimated ET_0 Séch versus the FAO-56 PM computation for each reference weather station.

The equation (5) is the final calibrated PM_{red} ET_0 method with all the calibrated coefficients. The input R_n term is deduced from the calibrated BC_{mod} R_S method (Eq. (4)).

$$ET_{0\ Séch} = 0.994 \frac{0.408\Delta(R_n - 0) + \gamma \frac{900}{T_{avg} + 273} 1.5(e_s - e_a)}{\Delta + \gamma(1 + 0.34\ 1.5)} + 0.013 \quad (5)$$

4.2. Recharge-area parameters

Sub-areas are expressed in percentages of the whole recharge area (Table 4 and Fig. 6). Two types of vegetation cover, pasture and forest, are defined using aerial photographs, with proportions of 23% and 53%, respectively. The Séchilienne forest is mainly composed of beeches (*Fagus sylvatica*) and conifers (*Picea excelsa*), which are associated occasionally with ashes (*Fraxinus*) and sweet chestnuts (*Castanea sativa*). Three main geology sub-areas, micaschist bedrock (15%), sedimentary cover (20%) and superficial formations (41%), are defined through examination of the geological map and field investigations. Infiltration structures are centered on the major faults identified on the geological map, on lineaments deduced from aerial-photograph analysis and on geomorphological features (sinkholes, cracks...). A 50-meter wide influence zone is added to the identified objects, leading to an infiltration-structure sub-area representing 24% of the recharge area.

For K_c estimation, the proportion of beeches and conifers is assumed to be identical for the Séchilienne forest (each 50% of forest sub-area) and other species are ignored. K_c are set to 0.71 and 0.97 for conifers, and to 0.78 and 0.9 for beeches according to Verstraeten et al. (2005). Most pastures are anthropogenic and consist of grass. K_c are set to 0.85 and 1 according to Allen et al. (1998). Infiltration structure sub-areas are not taken into account in the K_c estimation, so the relative proportions of pasture and forest become 30% and 70%, respectively. The contribution of each sub-area (Table 4, column "K_c RA") allows the determination of the recharge area K_c values at the scale of the recharge area (0.777 to 0.955).

The combination of geology and vegetation sub-areas results in six types of SAWC sub-areas (Table 4). For each SAWC sub-area, at least one auger hole was drilled. For each soil auger core, the soil texture, the stoniness and the organic-matter content are estimated by morphological description (Jabiol and Baize, 2011). Based on these estimations, the SAWC is then computed using the pedotransfer functions of Jamagne et al (1977) and Bruand et al. (2004). The average estimation of SAWC at the recharge area scale is 106 ±10 mm (rounded to 105 mm).

To estimate the R_{coeff}, an average slope gradient is computed from slope gradient analysis of the DEM and is assigned to each vegetation sub-area. Pasture and forest sub-areas show an average slope gradient of 14° and of 20.6° respectively. R_{coeff} values of 22% for pasture and 15% for forest are deduced from Sautier chart (Musy and Higy, 2011). This chart was developed for Switzerland where environmental conditions are similar to the French Alps. A 12.8% runoff coefficient is then estimated at the recharge area scale, according to the respective proportions of vegetation sub-areas (Table 4).

4.3. Sensitivity analysis of the parameters of the recharge area

Sensitivity analysis is performed for SAWC ranging from 0 (100% of infiltration structures corresponding to precipitation) to 145 mm of SAWC (0% infiltration structures +10 mm of SAWC uncertainties measurement) with increments of 10 mm. The coupled surface R_{coeff} ranges from 0 to 16.3% (with increments of about 1%). For each combination, recharge is computed according to the soil-water balance (Fig. 1 – Step 3 and Fig. 2) with: (i) the temperature estimated for the recharge area (Appendix B), (ii) the precipitation recorded at Mont-Sec weather station, and (iii) the parameters of the recharge area.

All the best computations have a one-day lag, with periods ranging from 56 to 104 days (Fig. 7A and Table 5). The best R^2 obtained from recharge is obtained with both the estimated recharge-area parameters (SAWC = 105 mm, $R^2 = 0.618$) and the recharge-area parameters for SAWC adjusted from 75 ($R^2 = 0.616$) to 115 mm ($R^2 = 0.617$, Fig. 7B and Table 5). One of the best correlation performances is obtained for the estimated recharge-area parameters. This shows that the delimitation of the recharge area properly reflects the actual field conditions. The best correlation performance is assumed to be obtained, with the estimated parameter-recharge parameters for the NH4 null hypothesis, i.e. testing R^2 obtained with the estimated recharge-area set (SAWC = 105 mm) minus R^2 obtained with each of the other adjusted recharge-parameter sets of the sensitivity analysis (Table 5).

For all the recharge combinations tested, the LBCI values from bootstrap testing of NH2 are greater than 0, allowing to reject the null hypothesis NH2 (Fig. 7C). In other words, it shows that the R^2 obtained with recharge is always significantly higher than the one computed with precipitation ($R^2 = 0.311$) even for a SAWC of 5 mm ($R^2 = 0.426$, Table 5). For the adjusted recharge-area parameters scenarios having SAWC values above 45 mm, the LBCI values from bootstrap testing of NH4 are lower than 0, not allowing to reject the null hypothesis NH4 (Table 5 and Fig. 7D). In other words, it shows that the R^2 obtained with a SAWC of 105 mm is not significantly higher than the ones obtained from SAWC above 45 mm. Recharge-displacement correlations for SAWC values ranging from 75 (runoff = 9%) to 115 mm (runoff = 13.9%) show (i) a cumulative period computation (n) below 101 days, that is within the third quartile, (ii) an R^2 greater than 0.616, that is within the third quartile, (iii) LBCI values of NH2 greater than 0 and (iv) LBCI values of NH4 lower than 0 (Table 5 and Fig. 7). These SAWC and runoff values seem to statistically reflect the recharge area properties of the landslide and are suggested for further work on the Séchilienne landslide.

4.4. Estimation of the recharge for the Séchilienne landslide

For the remaining part of this paper, the R_{LRIW} is based on the estimated recharge-area parameters (infiltration structures = 24%, SAWC = 105 mm, and R_{coeff} = 12.8%). Indeed, among all solutions giving satisfying performances in the sensitivity analysis, these parameters arise from actual field data. The R_{LRIW} is compared with the precipitation signal in Fig. 8.

The R_{LRIW} signal differs significantly from the precipitation signals, marked by a high seasonal contrast. This is especially true during summer when ET_c is important. Indeed, the first rainfall events after a dry period do not reach the aquifer until the SAWC is exceeded. Figure 9 shows the best correlation results for precipitation and $R_{LRIW,}$ together with A16 detrended daily displacements. The cumulative recharge signal reproduces well the displacement acceleration and deceleration phases, and especially the dry summers where displacement dramatically dropped (summers 1997, 1998, 2003, 2004 and 2009, Fig. 9B). On the contrary, the cumulative precipitation signal is more contrasted and more noisy, and does

not manage to reproduce several peaks (in width as well as in intensity) of the detrended displacement signal (winters 1997, 2000, 2004, 2005 and 2010). In addition, the cumulative precipitation signal shows a weak correlation with displacement deceleration phases (summers 1998, 1999, 2000 2006, 2009 and 2010).

5. Discussion

5.1. Relevance of the LRIW method

Figure 10 summarizes the comparison of the performances between the precipitation, the R_{PMNE} and the R_{LRIW} based on the NH1, NH2 and NH3 tests for the four extensometers. All LBCI values from bootstrap testing of NH1, NH2 and NH3 are greater than zero, allowing to reject the three null hypotheses for the four stations (Fig. 10A). Rejection of the NH1 null hypothesis shows that R^2 obtained with R_{PMNE} are significantly higher than those computed with precipitation. Rejection of the NH2 null hypothesis shows that the R^2 obtained with R_{LRIW} are significantly higher than those computed with precipitation. Similarly, rejection of the NH3 null hypothesis shows that R^2 obtained with R_{LRIW} are significantly higher than those computed with R_{PMNE}. R^2 values vary from 0.0006 to 0.343 for precipitation, from 0.076 to 0.444 for R_{PMNE} and from 0.243 to 0.586 for R_{LRIW}, for G5 and A16 extensometer respectively (Table 2). On average, R_{PMNE} allows to increase the R^2 value by 29% relatively to precipitation, while R_{LRIW} allows to increase the R^2 by 78% (Fig. 10B). The R^2 obtained with R_{LRIW} are 38% higher on average than those obtained with R_{PMNE}.

These results are confirmed by the LBCI and by the observed values of the NH2 test which are always greater than those from the NH1 test as well as by the positive LBCI values of the NH3 test (Fig. 10). The correlation performance for the recharge estimated with the LRIW method significantly exceeds the performances of the two other signals, making the LRIW method particularly appropriate to be used in landslide studies. A discussion about the benefit of this study for the understanding of the rainfall-displacement relationship in the case of the Séchilienne landslide can be found in appendix C.

5.2. Applicability of the LRIW method to other landslides

Several studies have shown the relevance of the recharge signal for various landslide types: coastal landslides (Maquaire, 2000; Bogaard et al., 2013), unstable embankment slope landslides (Cartier and Pouget, 1987; Delmas et al., 1987; Matichard and Pouget, 1988) and deep-seated earth flow landslides (Malet et al., 2003; Godt et al., 2006). In addition, destabilization of shallow landslides is known to be influenced by antecedent soil moisture and precipitation (Brocca et al., 2012; Garel et al., 2012; Ponziani et al., 2012). Recharge, which implicitly gathers antecedent soil moisture and precipitation, can be a significant parameter to consider.

Although the method proposed in this study has not yet been tested at other sites, there are several arguments which suggest its applicability elsewhere. First, the FAO Penman-Monteith method used in this study is considered worldwide as the evapotranspiration method standard (Allen et al., 1998; Shahidian et al., 2012). Several evapotranspiration methods were developed locally and many of them can be calibrated against reference methods in other contexts (Hargreaves and Allen, 2003; Yoder et al., 2005; Alkaeed et al., 2006; Igbadun et al., 2006; Trajkovic, 2007; Alexandris et al., 2008; López-Moreno et al., 2009; Sivaprakasam et al., 2011; Tabari and Talaee, 2011; Shahidian et al., 2012; Tabari et al., 2013). Otherwise, the Penman-Monteith or Hargreaves-Samani methods are recommended (Allen et al., 1998). Several solar radiation methods were developed and can be applied worldwide if locally

calibrated, allowing estimation of evapotranspiration from temperature alone (Allen et al., 1998; Almorox, 2011). Recharge-area parameters can be estimated locally or with local or global literature reference values. The use of global values will increase recharge estimation uncertainties. However, the implementation of a sensitivity analysis allows a refinement of recharge-area parameters in order to compensate for the lack of site-specific data. Pachepsky and Rawls (2004) developed pedotransfer functions to estimate SAWC for various regions of the world. R_{coeff} values from the widely used rational method can be applied, as well as most of the runoff coefficients from the literature (McCuen, 2005; Musy and Higy, 2011). In addition, pedotransfer functions can also be used for runoff estimation. Lastly, vegetation coefficients are available from local surveys (Gochis and Cuenca, 2000; Verstraeten et al., 2005; Hou et al., 2010), but can also be found in the literature for many species (Allen et al., 1998).

6. Conclusion and perspectives

A method based on a soil-water balance, named LRIW, is developed to compute recharge on a daily interval, requiring the characterization of evapotranspiration and parameters characterising the recharge area (soil-available water-capacity and runoff). A workflow is developed to compute daily groundwater recharge and requires the records of precipitation, air temperature, relative humidity, solar radiation and wind speed within or close to the landslide. The determination of the parameters of the recharge area is based on a spatial analysis requiring field observations and spatial datasets (digital elevation models, aerial photographs and geological maps). Once determined, the parameters are refined with a sensitivity analysis.

The method has been tested on the Séchilienne landslide. The tests demonstrate that the performance of the correlation with landslide displacement velocity data is significantly enhanced using the LRIW estimated recharge. The R^2 obtained with the LRIW recharge are 78% higher on average than those obtained with precipitation and are 38% higher on average than those obtained with recharge computed with a commonly used simplification in several landslide studies (recharge = precipitation minus non-calibrated ET_0). The sensitivity analysis of the LRIW workflow appears to be an appropriate alternative to estimate or to refine soil-water balance parameters of the recharge area, especially in the case of insufficient field investigations or in the absence of the necessary spatial dataset.

The LRIW workflow is developed to be as universal as possible in order to be applied to other landslides. The workflow is developed in order to be sufficiently simple to guide any non-hydrogeology specialist who intends to estimate the recharge signal in the case of rainfall-landslide displacement studies. Within this scope, a software is planned to be developed in the near future in order to provide a user-friendly tool for recharge estimation. In addition, the LRIW workflow also enables the reconstruction of retrospective time series for sites recently equipped with weather stations designed to measure a full set of parameters. A further step will have to account for the spatial and temporal variabilities of precipitation and recharge area properties, thus providing a better estimation of the recharge. In addition, taking recharge into account can assist in determining a warning rainfall threshold for the deep-seated slope movements.

Acknowledgments

This research was funded by the SLAMS program (Séchilienne Land movement: Multidisciplinary Studies) of the National Research Agency (ANR). The meteorological data were provided by MétéoFrance, LTHE, ONF and CEREMA Lyon. Aerial photographs and the digital elevation model were provided by IGN. Displacement data were supplied by CEREMA Lyon. The authors acknowledge the support of Jean-Pierre Duranthon and Marie-Aurélie Chanut from the CEREMA Lyon and Jean-Paul Laurent from the LTHE. Appreciation is also given to Eric Lucot of Chrono-Environnement for his kind advices for soil log interpretation and to Patrick Giraudoux for his support to implement bootstrap tests. Lastly, the authors thank Peter Milmo for English and technical proof reading.

References

Alexandris, S., Stricevic, R. and Petkovic, S.: Comparative analysis of reference evapotranspiration from the surface of rainfed grass in central Serbia, calculated with six empirical methods against the Penman–Monteith formula, European Water, 21/22, 17–28, 2008.

Alfonsi, P.: Relation entre les paramètres hydrologiques et la vitesse dans les glissements de terrains. Exemples de La Clapière et de Séchilienne, Revue Française de Géotechnique, (79), 3–12, 1997.

Alkaeed, O. A., Flores, C., Jinno, K. and Tsutsumi, A.: Comparison of Several Reference Evapotranspiration Methods for Itoshima Peninsula Area, Fukuoka, Japan, Memoirs of the Faculty of Engineering, Kyushu University, 66(1), 1–14, 2006.

Allen, R. E., Pereira, L. S., Raes, D. and Smith, M.: Crop evapotranspiration : guidelines for computing crop water requirements, FAO Irrigation and drainage paper 56., Food and Agriculture Organization of the United Nations, Rome., 1998.

Allen, R. G., Smith, M., Pereira, L. S. and Perrier, A.: An Update for the Definition of Reference Evapotranspiration, ICID Bulletin of the International Commission on Irrigation and Drainage, 43(2), 1–34, 1994.

Almorox, J.: Estimating global solar radiation from common meteorological data in Aranjuez, Spain, Turkish Journal of Physics, 35(1), 53–64, 2011.

Aragon, Y.: Séries temporelles avec R: Méthodes et cas, Springer Science & Business Media., 2011.

Van Asch, T. W. J., Buma, J. and van Beek, L. P. .: A view on some hydrological triggering systems in landslides, Geomorphology, 30(1–2), 25–32, doi:10.1016/S0169-555X(99)00042-2, 1999.

Belle, P., Aunay, B., Bernardie, S., Grandjean, G., Ladouche, B., Mazué, R. and Join, J.-L.: The application of an innovative inverse model for understanding and predicting landslide movements (Salazie cirque landslides, Reunion Island), Landslides, 1–13, doi:10.1007/s10346-013-0393-5, 2013.

Binet, S., Guglielmi, Y., Bertrand, C. and Mudry, J.: Unstable rock slope hydrogeology: insights from the large-scale study of western Argentera-Mercantour hillslopes (South-East France), Bulletin de la Société Géologique de France, 178(2), 159–168, doi:10.2113/gssgfbull.178.2.159, 2007a.

Binet, S., Mudry, J., Scavia, C., Campus, S., Bertrand, C. and Guglielmi, Y.: In situ characterization of flows in a fractured unstable slope, Geomorphology, 86(1–2), 193–203, doi:10.1016/j.geomorph.2006.08.013, 2007b.

Bogaard, T., Guglielmi, Y., Marc, V., Emblanch, C., Bertrand, C. and Mudry, J.: Hydrogeochemistry in landslide research: a review, Bulletin de la Société Géologique de France, 178(2), 113–126, doi:10.2113/gssgfbull.178.2.113, 2007.

Bogaard, T., Maharjan, L. D., Maquaire, O., Lissak, C. and Malet, J.-P.: Identification of Hydro-Meteorological Triggers for Villerville Coastal Landslide, in Landslide Science and Practice, edited by C. Margottini, P. Canuti, and K. Sassa, pp. 141–145, Springer Berlin Heidelberg. [online] Available from: http://link.springer.com.biblioplanets.gate.inist.fr/chapter/10.1007/978-3-642-31427-8_18 (Accessed 12 June 2014), 2013.

Bonzanigo, L., Eberhardt, E. and Loew, S.: Long-term investigation of a deep-seated creeping landslide in crystalline rock. Part I. Geological and hydromechanical factors controlling the Campo Vallemaggia landslide, Can. Geotech. J., 44(10), 1157–1180, doi:10.1139/T07-043, 2007.

Bristow, K. L. and Campbell, G. S.: On the relationship between incoming solar radiation and daily maximum and minimum temperature, Agricultural and Forest Meteorology, 31(2), 159–166, doi:10.1016/0168-1923(84)90017-0, 1984.

Brocca, L., Ponziani, F., Moramarco, T., Melone, F., Berni, N. and Wagner, W.: Improving Landslide Forecasting Using ASCAT-Derived Soil Moisture Data: A Case Study of the Torgiovannetto Landslide in Central Italy, Remote Sensing, 4(12), 1232–1244, doi:10.3390/rs4051232, 2012.

Bruand, A., Duval, O. and Cousin, I.: Estimation des propriétés de rétention en eau des sols à partir de la base de données SOLHYDRO : Une première proposition combinant le type d'horizon, sa texture et sa densité apparente, Etude et Gestion des Sols, 11, 3, 323–334, 2004.

Brückl, E. P.: Cause-Effect Models of Large Landslides, Natural Hazards, 23(2-3), 291–314, doi:10.1023/A:1011160810423, 2001.

Canuti, P., Focardi, P. and Garzonio, C.: Correlation between rainfall and landslides, Bulletin of Engineering Geology and the Environment, 32(1), 49–54, doi:10.1007/BF02594765, 1985.

Cappa, F., Guglielmi, Y., Soukatchoff, V. M., Mudry, J., Bertrand, C. and Charmoille, A.: Hydromechanical modeling of a large moving rock slope inferred from slope levelling coupled to spring long-term hydrochemical monitoring: example of the La Clapière landslide (Southern Alps, France), Journal of Hydrology, 291(1–2), 67–90, doi:10.1016/j.jhydrol.2003.12.013, 2004.

Cappa, F., Guglielmi, Y., Viseur, S. and Garambois, S.: Deep fluids can facilitate rupture of slow-moving giant landslides as a result of stress transfer and frictional weakening, Geophys. Res. Lett., 41(1), 61–66, doi:10.1002/2013GL058566, 2014.

Cartier, G. and Pouget, P.: Corrélation entre la pluviométrie et les déplacements de pentes instables, in 9th European conference on soil mechanics and foundation engineering, vol. 1, CRC Press, Dublin. [online] Available from: http://www.crcpress.com/product/isbn/9789061917229 (Accessed 2 April 2014), 1987.

Castellvi, F.: A new simple method for estimating monthly and daily solar radiation. Performance and comparison with other methods at Lleida (NE Spain); a semiarid climate, Theoretical and Applied Climatology, 69(3), 231–238, doi:10.1007/s007040170028, 2001.

Chanut, M.-A., Vallet, A., Dubois, L. and Duranthon, J.-P.: Mouvement de versant de Séchilienne : relations entre déplacements de surface et précipitations – analyse statistique, in Journées Aléa Gravitaire 2013, Grenoble, France., 2013.

Chernick, M. R.: Bootstrap methods: A guide for practitioners and researchers, Wiley-Interscience, Hoboken, N.J., 2008.

Cordeiro, C. and Neves, M.: The Bootstrap methodology in time series forecasting, in COMPSTAT 2006 - Proceedings in Computational Statistics, pp. 1067–1073, Springer, Italy, Rome. [online] Available from: http://www.springer.com.biblioplanets.gate.inist.fr/statistics/computational+statistics/book/978-3-7908-1708-9, 2006.

Cowpertwait, P. S. P. and Metcalfe, A.: Introductory Time Series with R, Édition : 2009., Springer-Verlag New York Inc., Dordrecht ; New York., 2009.

Crozier, M. J.: Landslides: Causes, consequences et environment, Croom Helm, London ; Dover, N.H., 1986.

Delmas, P., Cartier, G. and Pouget, G.: Méthodes d'analyse des risques liés aux glissements de terrain, Bulletin Liaison Laboratoire Ponts et Chaussées, 150/151, 29–38, 1987.

Diodato, N., Guerriero, L., Fiorillo, F., Esposito, L., Revellino, P., Grelle, G. and Guadagno, F. M.: Predicting Monthly Spring Discharges Using a Simple Statistical Model, Water Resources Management, 28(4), 969–978, doi:10.1007/s11269-014-0527-0, 2014.

Duranthon, J.-P., Effendiaz, L., Memier, M. and Previtali, I.: Apport des méthodes topographiques et topométriques au suivi du versant rocheux instable des ruines de Séchilienne, Association Francaise de Topographie, (94), 31–38, 2003.

Durville, J.-L., Kasperki, J. and Duranthon, J.-P.: The Séchilienne landslide: monitoring and kinematics, in First Italian Workshop on Landslides, vol. 1, pp. 174–180, Napoli, Italia., 2009.

Garel, E., Marc, V., Ruy, S., Cognard-Plancq, A.-L., Klotz, S., Emblanch, C. and Simler, R.: Large scale rainfall simulation to investigate infiltration processes in a small landslide under dry initial conditions: the Draix hillslope experiment, Hydrological Processes, 26(14), 2171–2186, 2012.

Gochis, D. and Cuenca, R.: Plant Water Use and Crop Curves for Hybrid Poplars, Journal of Irrigation and Drainage Engineering, 126(4), 206–214, doi:10.1061/(ASCE)0733-9437(2000)126:4(206), 2000.

Godt, J. W., Baum, R. L. and Chleborad, A. F.: Rainfall characteristics for shallow landsliding in Seattle, Washington, USA, Earth Surf. Process. Landforms, 31(1), 97–110, doi:10.1002/esp.1237, 2006.

Guglielmi, Y., Cappa, F. and Binet, S.: Coupling between hydrogeology and deformation of mountainous rock slopes: Insights from La Clapière area (southern Alps, France), Comptes Rendus Geoscience, 337(13), 1154–1163, doi:10.1016/j.crte.2005.04.016, 2005.

Guglielmi, Y., Vengeon, J. M., Bertrand, C., Mudry, J., Follacci, J. P. and Giraud, A.: Hydrogeochemistry: an investigation tool to evaluate infiltration into large moving rock masses (case study of La Clapière and Séchilienne alpine landslides), Bulletin of Engineering Geology and the Environment, 61(4), 311 – 324, 2002.

Guzzetti, F., Peruccacci, S., Rossi, M. and Stark, C. P.: The rainfall intensity–duration control of shallow landslides and debris flows: an update, Landslides, 5(1), 3–17, doi:10.1007/s10346-007-0112-1, 2008.

Hargreaves, G. H. and Allen, R. G.: History and Evaluation of Hargreaves Evapotranspiration Equation, Journal of Irrigation and Drainage Engineering, 129(1), 53–63, doi:10.1061/(ASCE)0733-9437(2003)129:1(53), 2003.

Hargreaves, G. and Samani, Z.: Reference Crop Evapotranspiration from Temperature, Applied Engineering in Agriculture, 1(2), 96–99, 1985.

Helmstetter, A. and Garambois, S.: Seismic monitoring of Séchilienne rockslide (French Alps): Analysis of seismic signals and their correlation with rainfalls, Journal of Geophysical Research, 115(F3), F03016, doi:10.1029/2009JF001532, 2010.

Hong, Y., Hiura, H., Shino, K., Sassa, K., Suemine, A., Fukuoka, H. and Wang, G.: The influence of intense rainfall on the activity of large-scale crystalline schist landslides in Shikoku Island, Japan, Landslides, 2(2), 97–105, doi:10.1007/s10346-004-0043-z, 2005.

Hou, L. G., Xiao, H. L., Si, J. H., Xiao, S. C., Zhou, M. X. and Yang, Y. G.: Evapotranspiration and crop coefficient of Populus euphratica Oliv forest during the growing season in the extreme arid region northwest China, Agricultural Water Management, 97(2), 351–356, doi:10.1016/j.agwat.2009.09.022, 2010.

Igbadun, H., Mahoo, H., Tarimo, A. and Salim, B.: Performance of Two Temperature-Based Reference Evapotranspiration Models in the Mkoji Sub-Catchment in Tanzania, Agricultural Engineering International: the CIGR Ejournal, VIII [online] Available from: http://ecommons.library.cornell.edu/handle/1813/10573 (Accessed 15 April 2014), 2006.

Itenfisu, D., Elliott, R. L., Allen, R. G. and Walter, I. A.: Comparison of Reference Evapotranspiration Calculations as Part of the ASCE Standardization Effort, Journal of Irrigation and Drainage Engineering, 129(6), 440–448, doi:10.1061/(ASCE)0733-9437(2003)129:6(440), 2003.

Jabiol, B. and Baize, D.: Guide pour la description des sols, Quae éditions., 2011.

Jacobson, P. M. Z.: Fundamentals of Atmospheric Modeling, Édition : 2., Cambridge University Press, Cambridge, UK; New York., 2005.

Jamagne, M., Bétrémieux, R., Bégon, J. C. and Mori, A.: Quelques données sur la variabilité dans le milieu naturel de la réserve en eau des sols, Bulletin Technique d'Information du Ministère de l'Agriculture, (324-325), 627–641, 1977.

Jensen, M. E., Burman, R. D. and Allen, R. G.: Evapotranspiration and irrigation water requirements : a manual, American Society of Civil Engineers, New York., 1990.

Lebrouc, V., Schwartz, S., Baillet, L., Jongmans, D. and Gamond, J. F.: Modeling permafrost extension in a rock slope since the Last Glacial Maximum: Application to the large Séchilienne landslide (French Alps), Geomorphology, 198, 189–200, doi:10.1016/j.geomorph.2013.06.001, 2013.

López-Moreno, J. I., Hess, T. M. and White, S. M.: Estimation of reference evapotranspiration in a mountainous mediterranean site using the Penman-Monteith equation with limited meteorological data, Pirineos, 164, 7–31, 2009.

Lu, J., Sun, G., McNulty, S. G. and Amatya, D. M.: A comparison of six potential evapotranspiration methods for regional use in the Southeastern United States, JAWRA Journal of the American Water Resources Association, 41(3), 621–633, doi:10.1111/j.1752-1688.2005.tb03759.x, 2005.

Madsen, H.: Time Series Analysis, 1 edition., Chapman and Hall/CRC, Boca Raton., 2007.

Makkink, G. .: Testing the Penman formula by means of lysimeters, Journal of the Institution of Water Engineers, 11, 277–288, 1957.

Malet, J. P., Maquaire, O. and Vanash, T. W.: Hydrological behaviour of earthflows developed in clay-shales: investigation, concept and modelling, The Occurrence and Mechanisms of Flows in Natural Slopes and Earthfills, Patron Editore, Bologna, 175–193, 2003.

Maquaire, O.: Effects of Groundwater on the Villerville-Cricqueboeuf Landslides , Sixteen Year Survey (Calvados, France), in 8th Landslides International symposium, pp. 1005–1010, Cardiff., 2000.

Matichard, Y. and Pouget, P.: Pluviométrie et comportement de versants instables, in Landslides : proceedings of the fifth International Symposium on Landslides, pp. 725–730, Lausanne, Switzerland., 1988.

McCuen, R. H.: Hydrologic analysis and design, Pearson Prentice Hall, Upper Saddle River, N.J., 2005.

Meric, O., Garambois, S., Jongmans, D., Wathelet, M., Chatelain, J. L. and Vengeon, J. M.: Application of geophysical methods for the investigation of the large gravitational mass movement of Séchilienne, France, Can. Geotech. J., 42(4), 1105–1115, doi:10.1139/t05-034, 2005.

Meric, O., Garambois, S. and Orengo, Y.: Large Gravitational Movement Monitoring Using a Spontaneous Potential Network, in Proc. 19th Annual Symposium on the Application of Geophysics to Engineering and Environmental Problems, pp. 202–209, EEGS, Seattle, USA., 2006.

Mudry, J. and Etievant, K.: Synthèse hydrogéologique du versant instable des Ruines de Séchilienne, Unpublished report, UMR Chrono-Environnement, University of Franche-Comté., 2007.

Musy, A. and Higy, C.: Hydrology: A Science of Nature, English ed., CRC Press ; Science Publishers, Boca Raton, FL. : Enfield, N.H., 2011.

Noverraz, F., Bonnard, C., Dupraz, H. and Huguenin, L.: Grands glissements de terrain et climat, VERSINCLIM - Comportement passé, présent et futur des grands versants instables subactifs en fonction de l'évolution climatique, et évolution en continu des mouvements en profondeur, Rapport final PNR31 (Programme National de Recherche), vdf Hochschulverlag AG an der ETH Zürich, Zürich, Switzerland., 1998.

Pachepsky, Y. and Rawls, W. J.: Development of pedotransfer functions in soil hydrology, Elsevier, Amsterdam; New York., 2004.

Patwardhan, A., Nieber, J. and Johns, E.: Effective Rainfall Estimation Methods, Journal of Irrigation and Drainage Engineering, 116(2), 182–193, doi:10.1061/(ASCE)0733-9437(1990)116:2(182), 1990.

Pisani, G., Castelli, M. and Scavia, C.: Hydrogeological model and hydraulic behaviour of a large landslide in the Italian Western Alps, Nat. Hazards Earth Syst. Sci., 10(11), 2391–2406, doi:10.5194/nhess-10-2391-2010, 2010.

Ponziani, F., Pandolfo, C., Stelluti, M., Berni, N., Brocca, L. and Moramarco, T.: Assessment of rainfall thresholds and soil moisture modeling for operational hydrogeological risk prevention in the Umbria region (central Italy), Landslides, 9(2), 229–237, doi:10.1007/s10346-011-0287-3, 2012.

Priestley, C. H. B. and Taylor, R. J.: On the Assessment of Surface Heat Flux and Evaporation Using Large-Scale Parameters, Monthly Weather Review, 100(2), 81–92, doi:10.1175/1520-0493(1972)100<0081:OTAOSH>2.3.CO;2, 1972.

Prokešová, R., Medveďová, A., Tábořík, P. and Snopková, Z.: Towards hydrological triggering mechanisms of large deep-seated landslides, Landslides, 10(3), 239–254, doi:10.1007/s10346-012-0330-z, 2013.

Rochet, L., Giraud, A., Antoine, P. and Évrard, H.: La déformation du versant sud du Mont-Sec dans le secteur des ruines de Séchilienne (Isère), Bulletin of the International Association of Engineering Geology, 50(1), 75–87, doi:10.1007/BF02594959, 1994.

Le Roux, O., Jongmans, D., Kasperski, J., Schwartz, S., Potherat, P., Lebrouc, V., Lagabrielle, R. and Meric, O.: Deep geophysical investigation of the large Séchilienne landslide (Western Alps, France) and calibration with geological data, Engineering Geology, 120(1–4), 18–31, doi:10.1016/j.enggeo.2011.03.004, 2011.

Rutqvist, J. and Stephansson, O.: The role of hydromechanical coupling in fractured rock engineering, Hydrogeology Journal, 11(1), 7–40, doi:10.1007/s10040-002-0241-5, 2003.

Shahidian, S., Serralheiro, R., Serrano, J., Teixeira, J., Haie, N. and Santos, F.: Hargreaves and Other Reduced-Set Methods for Calculating Evapotranspiration, in Evapotranspiration - Remote Sensing and Modeling, edited by A. Irmak, pp. 60–80, InTech, Rijeka, Croatia., 2012.

Sivaprakasam, S., Murugappan, A. and Mohan, S.: Modified Hargreaves equation for estimation of ETo in a Hot and Humid Location in Tamilnadu State, India, Int. Journal of Engineering Science and Technology, 3, 592–600, 2011.

Tabari, H., Grismer, M. E. and Trajkovic, S.: Comparative analysis of 31 reference evapotranspiration methods under humid conditions, Irrigation Science, 31(2), 107–117, doi:10.1007/s00271-011-0295-z, 2013.

Tabari, H. and Talaee, P. H.: Local Calibration of the Hargreaves and Priestley-Taylor Equations for Estimating Reference Evapotranspiration in Arid and Cold Climates of Iran Based on the Penman-Monteith Model, Journal of Hydrologic Engineering, 16(10), 837–845, doi:10.1061/(ASCE)HE.1943-5584.0000366, 2011.

Trajkovic, S.: Temperature-Based Approaches for Estimating Reference Evapotranspiration, Journal of Irrigation and Drainage Engineering, 131(4), 316–323, doi:10.1061/(ASCE)0733-9437(2005)131:4(316), 2005.

Trajkovic, S.: Hargreaves versus Penman-Monteith under Humid Conditions, Journal of Irrigation and Drainage Engineering, 133(1), 38–42, doi:10.1061/(ASCE)0733-9437(2007)133:1(38), 2007.

Trajkovic, S. and Stojnic, V.: Effect of wind speed on accuracy of Turc method in a humid climate, Facta universitatis - series: Architecture and Civil Engineering, 5(2), 107–113, doi:10.2298/FUACE0702107T, 2007.

Turc, L.: Evaluation des besoins en eau d'irrigation, évapotranspiration potentielle, formule simplifiée et mise à jour., Annales Agronomiques, 12, 13–49, 1961.

Vengeon, J. M.: Déformation et rupture des versants en terrain métamorphique anisotrope: Apport de l'étude des Ruines de Séchilienne, PhD thesis, Université Joseph Fourier I, Grenoble, 3 November., 1998.

Verstraeten, W. W., Muys, B., Feyen, J., Veroustraete, F., Minnaert, M., Meiresonne, L. and De Schrijver, A.: Comparative analysis of the actual evapotranspiration of Flemish forest and cropland, using the soil water balance model WAVE, Hydrol. Earth Syst. Sci., 9(3), 225–241, doi:10.5194/hess-9-225-2005, 2005.

Yoder, R. E., Odhiambo, L. O. and Wright, W. C.: Evaluation of methods for estimating daily reference crop evapotranspiration at a site in the humid Southeast United States, Applied Engineering in Agriculture, 21(2), 197–202, 2005.

Zêzere, J. L., Trigo, R. M. and Trigo, I. F.: Shallow and deep landslides induced by rainfall in the Lisbon region (Portugal): assessment of relationships with the North Atlantic Oscillation, Natural Hazards and Earth System Sciences, 5(3), 331–344, doi:10.5194/nhess-5-331-2005, 2005.

Appendix A: Equations for evapotranspiration and solar radiation methods

A.1 Equation parameters terms for all equations

R_a	extraterrestrial solar radiation [MJ m^{-2} day^{-1}]
R_s	solar radiation [MJ m^{-2} day^{-1}]
R_n	net solar radiation [MJ m^{-2} day^{-1}]
N	maximum possible duration of sunshine [hour]
n	actual daily duration of sunshine [hour]
T_{avg}	average air temperature at 2 m height [°C]
T_{min}	minimum air temperature at 2 m height [°C]
T_{max}	maximum air temperature at 2 m height [°C]
G	soil heat flux density [MJ m^{-2} day^{-1}]
γ	psychrometric constant [kPa $°C^{-1}$]
u_2	wind speed at 2 m height [m s^{-1}]
e_s	mean saturation vapour pressure [kPa]
e_a	actual vapour pressure [kPa]
e^o	saturation vapour pressure at the air temperature T [kPa]
Δ	slope of vapour pressure curve [kPa $°C^{-1}$]
RH	relative humidity [%]
α	cloud cover adjustment factor [unitless]

The procedure for calculating these equation terms are given in the FAO-56 guidelines for computing crop water requirements (Allen et al., 1998).

A.2 Solar radiation (R_S)

The solar radiation $BC\ R_s$ is obtained from the Bristow-Campbell method (Bristow and Campbell, 1984):

$$BC\ R_s = A_{BC}\ Ra\left[1 - exp\left(-B_{BC}\left(\alpha\ \Delta T_{BC}\right)^{C_{BC}}\right)\right] \text{with } \Delta T_{BC} = T_{max(j)} - \frac{T_{\min(j)} + T_{\min(j+1)}}{2} \quad \text{(A1)}$$

The solar radiation $HS\ R_s$ obtained from the Hargreaves-Samani method (Hargreaves and Samani, 1985):

$$HS\ R_s = A_{HS} Ra\left(\Delta T_{HS}\right)^{B_{HS}} \text{ with } \Delta T_{HS} = T_{max(j)} - T_{\min(j)} \quad \text{(A2)}$$

where:

j is for the current target day and j+1 is for the following day

A_{BC}, B_{BC}, C_{BC} are the Bristow-Campbell empirical coefficients (no default values)

A_{HS}, B_{HS} are the Hargreaves-Samani empirical coefficients ($A_{HS} = 0.16$ *and* $B_{HS} = 0.5$)

In this study, the modified forms of R_S equation of Bristow-Campbell and Hargreaves-Samani are implemented: (i) a constant is added to take into account the possibility of a R_S estimation shift, (ii) the ΔT from the Bristow-Campbell method is used in both equations, and (iii) a cloud cover adjustment factor α is applied to ΔT since, for cloudy conditions, ΔT can produce an estimate larger than the incoming solar radiation (Bristow and Campbell, 1984).

Bristow-Campbell modified equation ($BC_{mod}\ R_s$):

$$BC_{mod}\ R_s = A_{BC}\ Ra\left[1 - exp\left(-B_{BC}\ \left(\alpha\ \Delta T\right)^{C_{BC}}\right)\right] + D_{BC} \quad \text{(A3)}$$

Hargreaves-Samani modified equation ($HS_{mod}\ R_s$):

$$HS_{mod}\ R_s = A_{HS}\ Ra\left(\alpha\ \Delta T\right)^{B_{HS}} + C_{HS} \quad \text{(A4)}$$

with $\Delta T = T_{max(j)} - \frac{T_{\min(j)} + T_{\min(j+1)}}{2}$

where:

j is for the current day and j+1 is for the following day

$A_{BC}, B_{BC}, C_{BC}, D_{BC}$ are the Bristow-Campbell regional calibration coefficients

A_{HS}, B_{HS}, C_{HS} are the Hargreaves-Samani regional calibration coefficients

The α coefficient is applied for the two first rain-event days since, for a rain period longer than two days, the value of the Rs estimated from ΔT and the actual R_S value become almost identical. If ΔT on the day before a rain event (ΔT_{j-1}) is less than ΔT_{j-2} by more than 2°C, the coefficient α is also applied assuming that cloud cover was already significantly present. For the remaining days, α is not applied (α = 1). A 2°C threshold and a 2-day period is used

(Bristow and Campbell, 1984). In this study, the calibration of α is based on the principle that if this adjustment is not relevant, a calibrated α coefficient would be equal to 1 (no effect).

R_S can also be calculated with the Angström formula using sunshine duration data recorded at a weather station (FAO-56 guidelines, Allen et al., 1998):

$$R_s = \left(a_s + b_s \frac{n}{N} \right) R_a \tag{A5}$$

where: $a_s + b_s$ is the fraction of extraterrestrial solar radiation reaching the Earth surface on clear days (default values, a_s=0.25 and b_s = 0.5).

A.3 Reference vegetation evapotranspiration (ET_0)

The reference vegetation evapotranspiration $FAO-56\,PM\;ET_0$ obtained from the Penman-Monteith method modified form from the FAO paper number 56 (Allen et al., 1998) is:

$$FAO-56\,PM\;ET_0 = \frac{0.408\Delta\left(R_n - G\right) + \gamma \frac{900}{T_{avg}+273} u_2 \left(e_s - e_a\right)}{\Delta + \gamma\left(1 + 0.34 u_2\right)} \tag{A6}$$

The reference vegetation evapotranspiration $HS\,ET_0$ obtained from the Hargreaves-Samani method (Hargreaves and Samani, 1985) is:

$$HS\,ET_0 = 0.0135\ 0.408\,Rs\left(T_{avg} + 17.8\right) \tag{A7}$$

The unit conversion factor 0.408 is added to the original formula in order to compute ET_0 in mm day^{-1} with R_S in MJ m^{-2} day^{-1}.

The reference vegetation evapotranspiration $Turc\,ET_0$ obtained from the Turc method (Turc, 1961) is:

$$For\ RH > 50\%, \quad Turc\,ET_0 = 0.01333 \frac{T_{avg}}{T_{avg}+15}\left(23.9001\,Rs + 50\right) \tag{A8}$$

$$For\ RH < 50\%, \quad Turc\,ET_0 = 0.01333 \frac{T_{avg}}{T_{avg}+15}\left(23.9001\,Rs + 50\right)\left(1 + \frac{50 - RH}{70}\right) \tag{A9}$$

For the Séchilienne landslide, the equation (A8) is preferred to the equation (A9) because of an average relative humidity (RH) of the nearby mountain weather stations greater than 50% (Chamrousse, 70%; Saint-Michel-Maur, 66 %; Saint-Jean-Saint-Nicolas, 66 %).

The reference vegetation evapotranspiration $PT\,ET_0$ obtained from the Priestley-Taylor method (Priestley and Taylor, 1972) is:

$$PT\ ET_0 = 1.26 \frac{\Delta}{\Delta + \gamma}\left(R_n - G\right) \tag{A10}$$

The reference vegetation evapotranspiration $M\,ET_0$ obtained from the Makkink method (Makkink, 1957) is:

$$M\ ET_0 = 0.61 \frac{\Delta}{(\Delta + \gamma)} \frac{R_s}{2.45} - 0.012 \quad \text{(A11)}$$

The Penman-Monteith reduced-set method which allows to calculate the reference vegetation evapotranspiration $PM_{red}\,ET_0$ is identical to the PM FAO-56 method (Eq. (A6)), but humidity and wind speed are estimated according to FAO-56 guidelines (Allen et al., 1998). The actual vapour pressure is estimated with the equation (A12):

$$e_a = e^0(T_{min}) = 0.611\ exp\left(\frac{17.27\ T_{min}}{T_{min} + 237.3}\right) \quad \text{(A12)}$$

In the case of the Séchilienne landslide, the wind speed is fixed at 1.5 m/s at a 2-meter height (2 m/s by default), which is the daily average of the nearby mountain weather stations (Chamrousse, 2.33 m/s; Saint-Michel-Maur, 0.95 m/s; Saint-Jean-Saint-Nicolas, 1.26 m/s).

A.4 Practical informations

The ET_0 methods used in this study were developed for irrigation scheduling, for which the scope of application involves positive temperatures (plant water supply during the spring-summer growing period). However, in mountainous sites, winter temperatures are often below 0°C, and ET_0 empirical methods can compute negative ET_0 values. Negative ET_0 computed values do not have any physical meaning and are therefore set to zero for this study.

The Priestley-Taylor and Penman-Monteith ET_0 methods use net solar radiation (R_n) instead of R_S, which can be deduced from R_S following the FAO-56 guideline (Allen et al., 1998).

ET_0 reduce-set methods do not take into account the wind speed variations. By removing saturated air from the boundary layer, wind increases evapotranspiration (Shahidian et al., 2012). Several studies show the influence of the wind speed on ET_0 method performance and therefore on calibration (Itenfisu et al., 2003; Trajkovic, 2005; Trajkovic and Stojnic, 2007). For this study, the days with average wind speed above the 95th percentile of the dataset (extreme values) are disregarded for the calibration.

Appendix B: Temperature estimation at the Mont-Sec weather station

B.1 Method

The temperatures at the Mont-Sec weather station are estimated with the characterisation of the local air temperature gradient using two surrounding weather stations recording the temperatures at a daily rate (Luitel et La Mure weather stations). Once the local air temperature gradient is characterized, one of the station is used to estimate the Mont-Sec temperatures.

The decrease in air density with elevation leads to a decrease in air temperature known as the lapse rate (Jacobson, 2005). A commonly used value of this rate is -6.5 °C / 1000 m. The air temperature can thus be related to elevation. In order to compute a local air temperature gradient, two weather stations surrounding the Séchilienne site are used: Luitel and La Mure (Table 1 and Fig. 3). The Luitel station is located on the Séchilienne massif whereas the La Mure station is located about 18 km from the landslide. Both stations have weather conditions similar to the Séchilienne recharge area. Although, the temperature estimation from the Luitel station would probably be more accurate, in order to maximize common interval lengths of temperatures with displacement records from 1994 to 2012, the La Mure station with records from 1992 to 2012 is preferred to estimate temperatures at Mont-Sec.

The local air temperature gradient in relation to elevation is defined by Equation (B1). The La Mure station temperatures (minimum and maximum) are used to estimate the temperatures at Luitel in relation to elevation, over their common recording period. A linear regression between temperatures measured at La Mure and Luitel is performed to determine the *a* and *b* coefficients. The b coefficient, which gathers the lapse rate (λ) and the elevation difference, is then divided by the elevation difference of the two stations used for the calibration.

$$T_{(Station)} = a\,T_{(Mure)} + b = a\,T_{(Mure)} + \lambda\,Diff_{elevation}$$
$$\text{with } Diff_{elevation} = Elevation_{Mure} - Elevation_{Station} \quad \text{(B1)}$$

where:

a and b	regional calibration coefficients
T	temperature minimum or maximum [°C]
λ	temperature lapse rate [°C m^{-1}]
$Diff_{elevation}$	difference of elevation between two weather stations [m]
Elevation	weather station elevation [m asl]
Station	target station (Luitel for calibration, Mont-Sec for computation)

B.2 Results

The recording period used for temperature calibration is from 06 July 2006 to 23 July 2012 (2193 records). This is a common data interval for the two weather stations used (La Mure and Luitel). The estimation of the local air temperature gradient shows a very good performance with R^2 equal to 0.895 (LBCI at 5% level = 0.826) and 0.916 (LBCI at 5% level

= 0.850), and RMSE equal to 2.12 and 2.48 respectively for minimum and maximum daily temperature calibration. The equations (B2) and (B3) are used to estimate temperatures at Mont-Sec with temperatures measured at La Mure. Rather than taking the elevation of the Mont-Sec weather station (1147 m), the average elevation of recharge area (1200 m) is used, resulting in a difference of elevation with La Mure of 319 m. The estimated local air temperature gradient is 0.7°C per 100 meters of elevation (the average of the λ of the two following equations).

$$T_{min(\text{Mont Sec})} = 0.911\ T_{min(\text{Mure})} - 0.0056 \times 319 \quad \text{(B2)}$$

$$T_{max(\text{Mont Sec})} = 0.928\ T_{max(\text{Mure})} - 0.0087 \times 319 \quad \text{(B3)}$$

Appendix C: Rainfall-displacement relationship in the case of the Séchilienne landslide

The rainfall-displacement relationship is hereafter discussed for the precipitation and the R_{LRIW} signals. Although the R^2 values are significantly variable from one station to another, the 2.5^{th} and 97.5^{th} percentiles and the observed value of the NH2 test are rather constant for the four displacement stations (respectively about 0.145, 0.250 and 0.325, Fig. 10A). These results show that the improvement of the correlation performance by using recharge rather than precipitation has the same order of magnitude for the four stations, whereas R^2 values vary considerably between the four stations. This may be explained by the fact that groundwater hydrodynamics probably triggers the entire Séchilienne landslide while the displacement velocity response depends on the damage level of the rock at the location of the displacement station. This interpretation is supported by the variability of the cumulative period, the shift factor, the weighting factor and the R^2 value, especially between G5 and the three others stations (Table 2).

The cumulative period and the shift factor deduced from the antecedent cumulative sum allow to determine the response-time of the Séchilienne landslide to rainfall events. Displacement stations located in the high motion zone show homogenous time delays with shift factors of 2 to 3 days. The average cumulative periods beyond which precipitation or R_{LRIW} have no longer any influence on the landslide destabilisation are estimated at about 50 days for precipitation and 75 days for R_{LRIW}. The station G5 shows significantly different time delays and cumulative periods, whatever the precipitation or R_{LRIW} data used. This difference can be explained by the low signal-to-noise ratio which makes the correlations difficult to interpret.

Concerning the A16 extensometer, regarding precipitation R^2 is better for the recent-short testing interval (0.343) than for the former-long interval of the sensitivity analysis (0.311). Conversely, regarding the recharge, R^2 is better for the former-long interval (0.618) than for the recent-short testing interval (0.586). This could be the consequence of a degradation of the near-surface rock mechanical properties of the Séchilienne landslide (as suggested by the displacement trend, Fig. 4), which makes the landslide more sensitive to precipitation events in the recent period.

Lastly, the best correlations from the sensitivity analysis suggest that infiltration structures could gather a large proportion of the flow (up to 68% for SAWC = 45 mm; NH4 LBCI <0) with respect to their recharge surface area (24%, Table 5). If so, fractures can play an important role in the groundwater drainage from the massif towards the landslide aquifers.

Table 1: Summary of weather datasets with parameters used (●) at the various locations. Distance is the measured from the Séchilienne landslide, R_S is the solar radiation, N is the sunshine duration, W is the wind speed, H is the humidity, T is the temperature and P is the precipitation depth

Station Name	Elevation (m asl)	Distance (km)	From	To	R_S	N	W	H	T	P	Number of days with data
Saint-Jean-Saint-Nicolas	1210	55	01 Jan. 2004	01 Jan. 2012	●	●	●	●	●		2876
Saint-Michel-Maur	698	54	01 Jan. 2004	01 Jan. 2012		●	●	●	●		2864
Grenoble-Saint-Geoirs	384	51	08 Jul. 2009	01 Jan. 2012	●	●	●	●	●		907
Chamrousse	1730	9	12 Sep. 2002	01 Mar. 2012			●	●			3261
La Mure	881	18	9 Sep. 1992	01 Jan. 2012					●		7517
Luitel	1277	4	06 Jul. 2006	23 Jul. 2012					●		2193
Mont-Sec	1148	0.2	9 Sep. 1992	01 Jan. 2012						●	7517

Table 2: Statistics of the displacement records and results of the best linear correlation between precipitation/R_{LRIW} and displacement records for 4 displacement stations (1101, A13, A16 and G5). The displacement column indicates basic statistics of the displacement records: 1st quartile (Q1), median and 3rd quartile (Q3). Cumulative period (n), shift factor (β) and weighting factor (α) are the terms of the equation (3). P stands for precipitation, R_1 stands for R_{PMNE} and R2 stands for R_{LRIW}.

Station	Displacement mm/day	Cumulative period (n)			Shift factor (β)			Weighting factor (α)			R^2		
	Q1/median/Q3	P	R_1	R_2	P	R_1	R_2	P	R_1	R_2	P	R_1	R_2
1101	1.75 / 2.50 / 3.84	42	54	68	2	2	2	0.071	0.065	0.091	0.28	0.35	0.50
A13	1.18 / 1.75 / 3.41	52	80	82	3	2	2	0.102	0.070	0.091	0.28	0.37	0.52
A16	1.94 / 2.98 / 4.39	64	71	76	2	2	2	0.163	0.125	0.168	0.34	0.44	0.59
G5	0.02 / 0.05 / 0.08	8	169	132	0	6	6	0.039	0.003	0.011	0.001	0.08	0.24

Table 3: Calibration and performance of the five tested ET_0 methods relatively to the FAO-56 PM ET_0 standard (Penman-Monteith method defined in the FAO-56 paper). All the ET_0 methods are detailed in the appendix A. a, b and R^2 are the results of linear regression between FAO-56 PM ET_0 and tested ET_0 methods. RMSE is the root mean square error

Method	a	b	R^2	RMSE
HS Et_0	0.920	0.130	0.917	0.548
Turc ET_0	0.880	0.434	0.900	0.588
PS ET_0	0.352	0.365	0.919	0.533
M ET_0	1.107	-0.018	0.910	0.565
PM_{red} ET_0	0.994	0.013	0.932	0.505

Table 4: Estimation of Kc (vegetation coefficient), SAWC (soil available water capacity) and runoff for the recharge area of the Séchilienne landslide. Geology and vegetation are the sub-area factors identified and expressed in proportion of the recharge area. The average slope gradient is the slope gradient for each identified vegetation sub-area factor. Kc, R_{coeff} and SAWC columns are the estimated values for each sub-area factor. Kc RA, SAWC RA and R_{coeff} RA columns are the contribution of each sub-area parameter at the scale of the recharge area. The recharge-area bottom-row stands for the estimation at the scale of the recharge area

Geology sub-area (%)		Vegetation sub-area (%)	Average slope gradient (°)	Kc min. max.	Kc RA min. max.	R_{coeff} (%)	R_{coeff} RA (%)	SAWC (mm)	SAWC RA (mm)
Micaschist	3	Pasture 23	14.0	0.85 1	0.256 0.301	22	5.1	173	5
Sedimentary	9							100	9
Superficial formations	11							112	12
Micaschist	12	Forest 53	20.6	0.745 0.935	0.521 0.654	15	7.7	254	30
Sedimentary	11							81	9
Superficial formations	30							133	41
Outcrop no soil	24	24	-	-	-	0	0	0	0
Recharge area	100	100	-	-	0.777 0.955	-	12.8	-	106

Table 5: Sensitivity analysis results of the best correlation between precipitation/R_{LRIW} and A16 extensometer detrended displacement. IS is for infiltration structures. SAWC is the soil-available water-capacity. LBCI is the lower bound of the confidence interval. R^2 row is the R^2 computed from recharge-area parameters indicated in each table row. Cumulative period (n), shift factor (β) and weighting factor (α) are the terms of the equation (3). Null hypothesis NH2 test: R^2_{row}-$R^2_{precipitation}$. Null hypothesis NH4 test: $R^2_{SAWC\ 105}$-R^2_{row}

SAWC mm	R_{coeff} %	IS %	Cumulative Period (n) day	Shift factor (β) day	Weighting factor (α)	R^2	LBCI of R^2	LBCI of NH2	LBCI of NH4
0	0.0	100	56	1	0.1697	0.311	0.230	0	0.241
5	0.6	96	92	1	0.1362	0.426	0.335	0.073	0.139
15	1.8	89	101	1	0.1226	0.522	0.435	0.158	0.055
25	3.0	82	104	1	0.1259	0.563	0.481	0.194	0.022
35	4.2	75	104	1	0.1317	0.585	0.508	0.214	0.005
45	5.4	68	103	1	0.1374	0.599	0.525	0.227	-0.004
55	6.6	61	102	1	0.143	0.608	0.537	0.234	-0.008
65	7.8	53	101	1	0.1484	0.613	0.544	0.238	-0.009
75	9.0	46	100	1	0.155	0.616	0.548	0.240	-0.009
85	10.3	39	98	1	0.1609	0.618	0.551	0.242	-0.007
95	11.5	32	94	1	0.1648	0.618	0.552	0.242	-0.004
105	12.8	24	92	1	0.1689	0.618	0.552	0.241	0.000
115	13.9	18	89	1	0.1727	0.617	0.551	0.240	-0.002
125	15.1	10	86	1	0.1745	0.614	0.549	0.237	-0.003
135	16.3	3	82	1	0.1746	0.611	0.545	0.235	-0.003
145	16.3	-	77	1	0.1731	0.609	0.543	0.234	-0.003

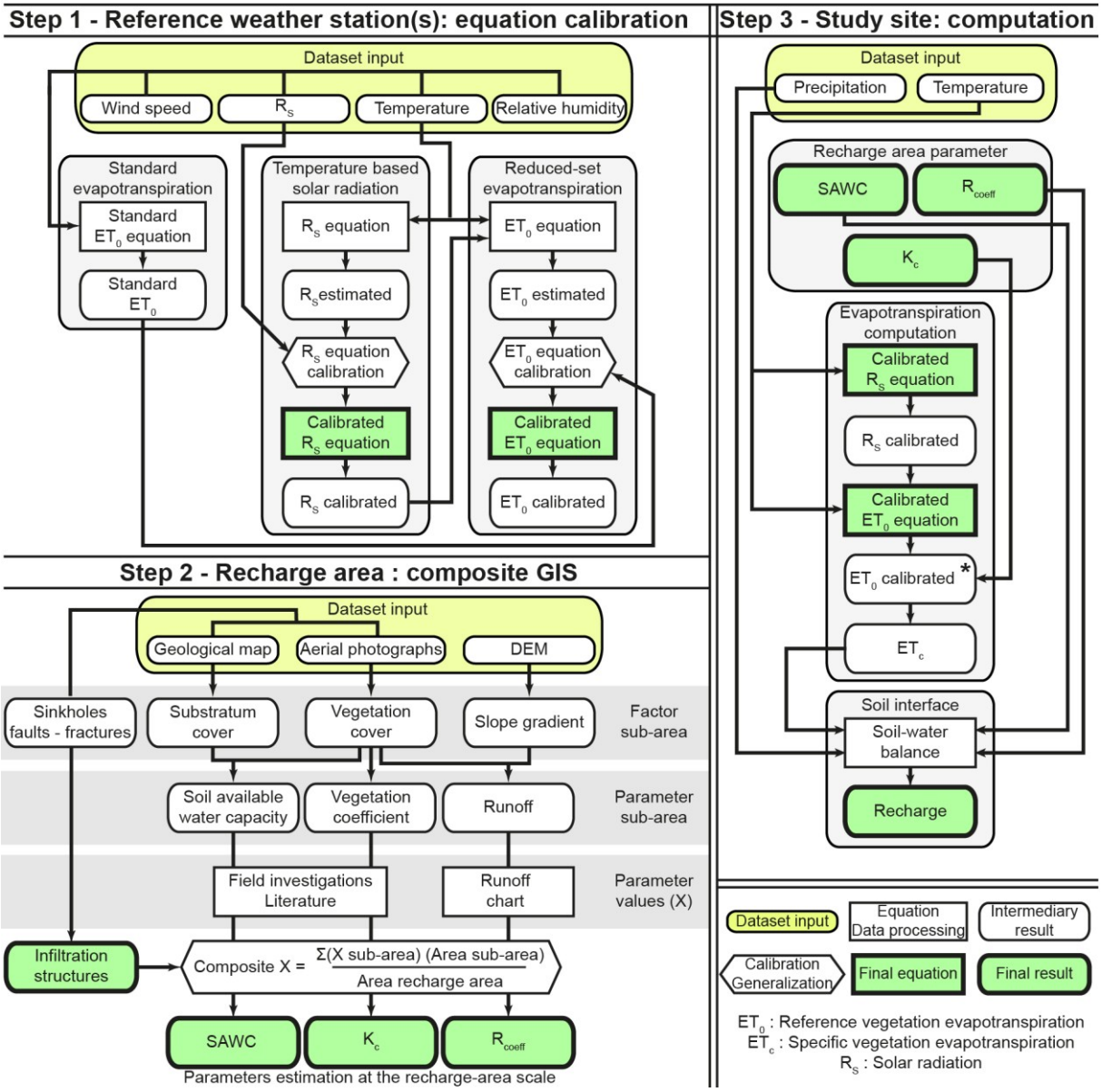

Fig. 1: Landslide Recharge Input Workflow (LRIW) diagram. Step 1: calibration of standard ET_0 and R_S methods. Step 2: estimation of recharge-area parameters required for the soil-water balance (R_{coeff}, K_c and SAWC) and the infiltration structures. Step 3: computation of the recharge with the soil-water balance. * In the case of a landslide-located weather station recording the full set of parameters, the first step can be skipped and the ET_0 of step 3 can be estimated directly at the study site with the standard ET_0 method (FAO-56 PM method)

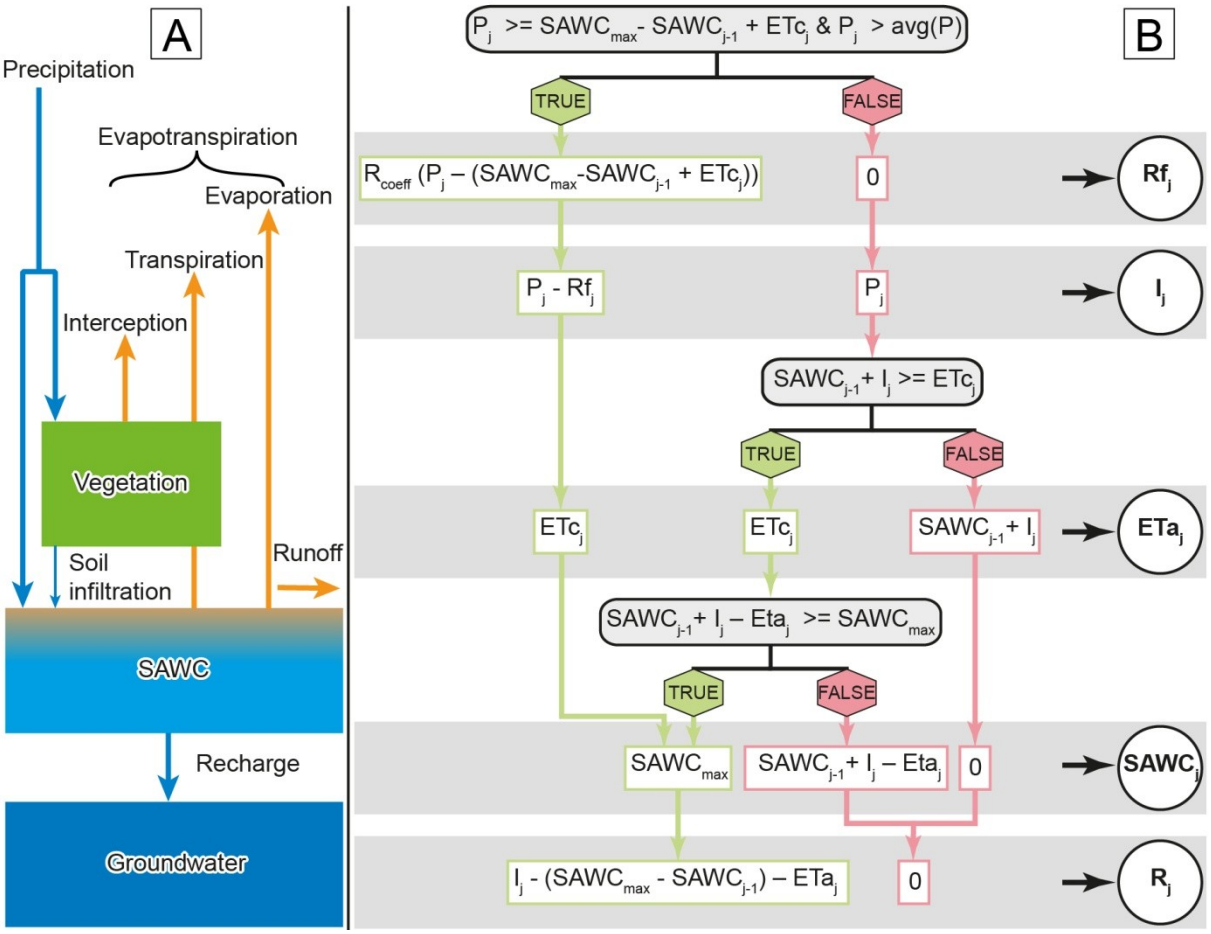

Fig. 2: Soil-water balance: (A) soil-water balance conceptual representation and (B) soil-water balance diagram used for recharge computation on a daily frequency. SAWC: soil-available water-capacity, $SAWC_{max}$: SAWC threshold (possible maximum), P: precipitation (rainfall + snow melt), avg (P): precipitation average of the entire record, I: part of precipitation which infiltrate the soil, Rf: surface runoff, R_{coeff}: runoff coefficient, ET_c: specific vegetation evapotranspiration, ET_a: actual vegetation evapotranspiration, and R: recharge. Units: mm of water, except R_{coeff} in percent. Subscript j is the computation day and subscript j-1 is the day before. TRUE and FALSE are the answers of the conditional inequality statements

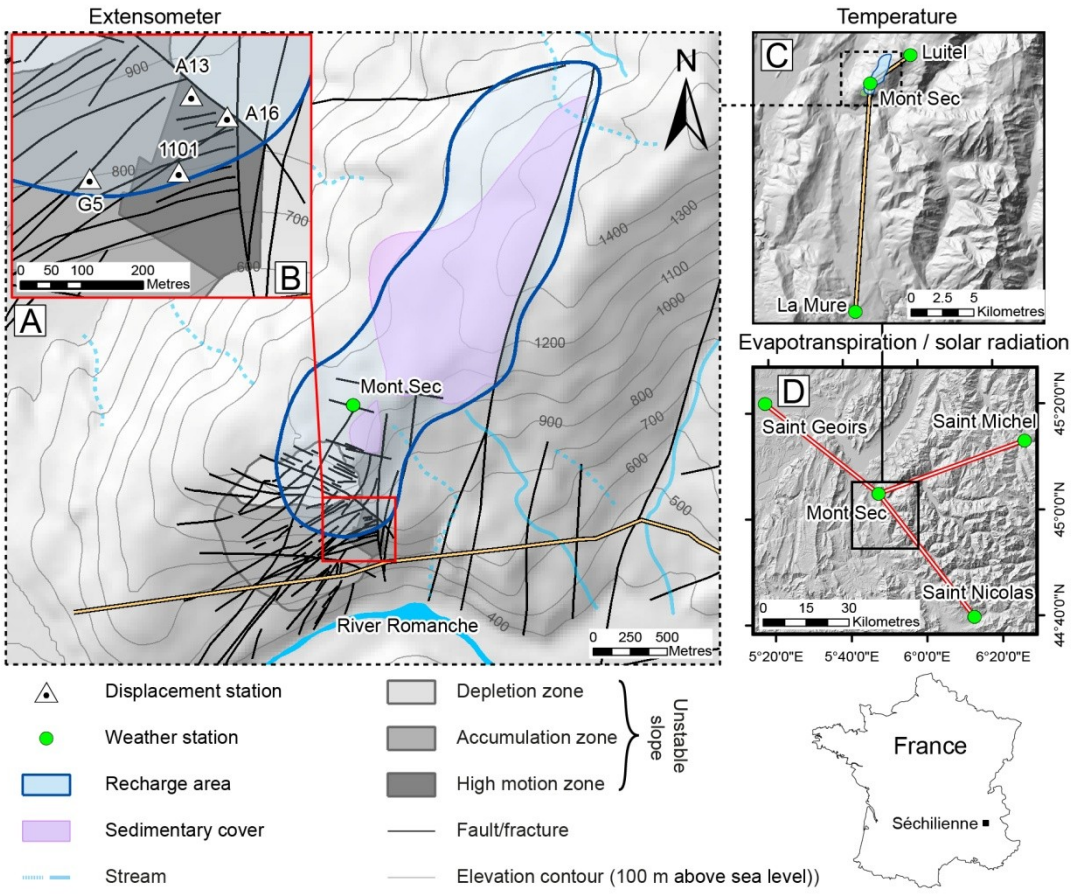

Fig. 3: Location map of the Séchilienne landslide. A: Map of the Séchilienne unstable slope and recharge area with Mont-Sec weather station. B: Enlarged map of the most active area showing displacement stations. C: Map showing the weather stations used for the temperature estimation at Mont-Sec. D: Map showing the weather stations used for evapotranspiration and solar radiation method calibration

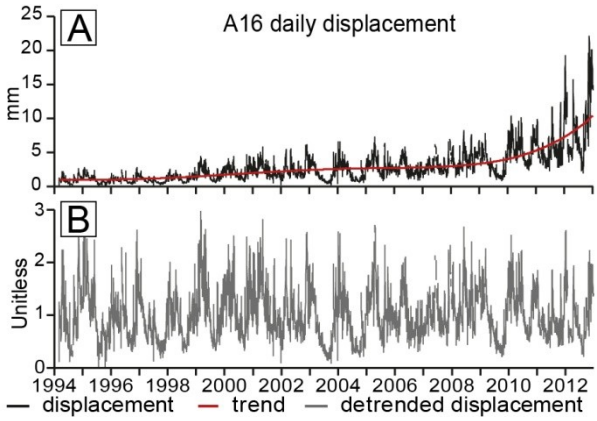

Fig. 4: Trend removal of A16 extensometer displacement data. A: A16 displacement data and the fourth order polynomial curve fitting considered as the displacement trend; B: A16 detrended data (unitless) corresponding to A16 displacement data for which the trend is removed by a multiplicative method

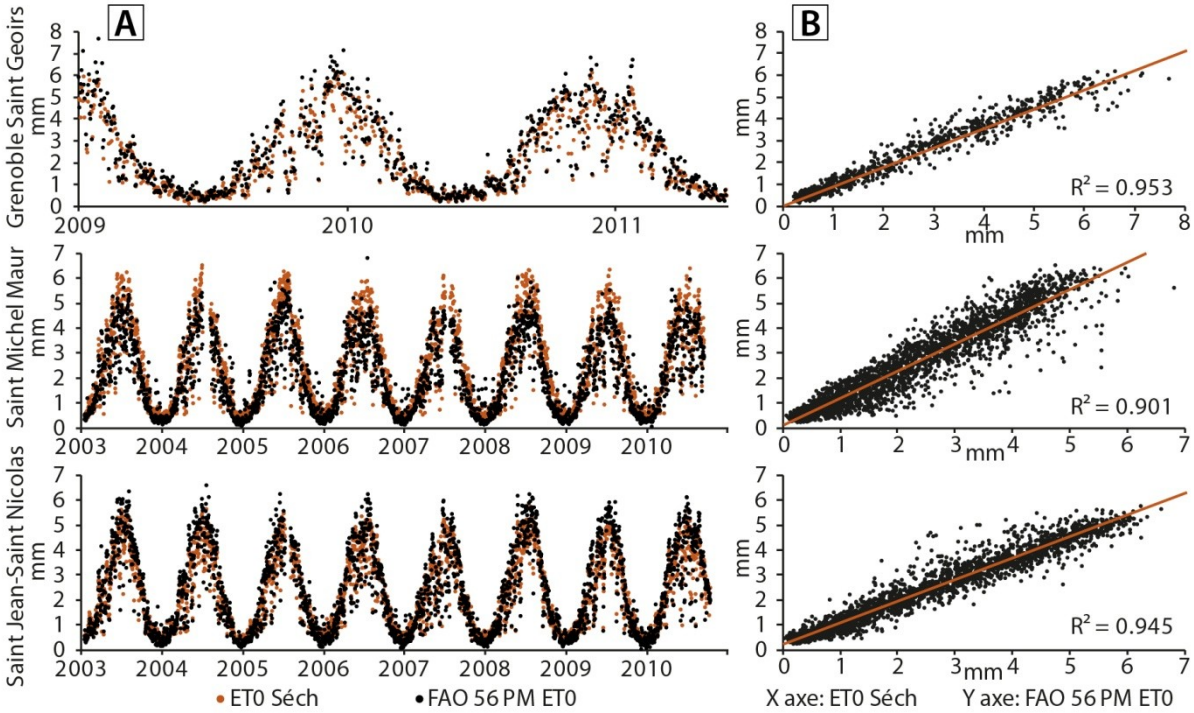

Fig. 5: ET_0 regional calibration results at the three reference weather stations (Grenoble-Saint-Geoirs, Saint-Jean-Saint-Nicolas and Saint-Michel-Maur). A: $ET_{0\ Séch}$ and FAO-56 PM ET_0 as a function of time. B: linear regression between $ET_{0\ Séch}$ (X axis) and FAO-56 PM ET_0 (Y axis). $ET_{0\ Séch}$ stands for ET_0 computed with the combination of calibrated ET_0 Penman-Monteith reduced-set method and calibrated R_S modified Bristow-Campbell method

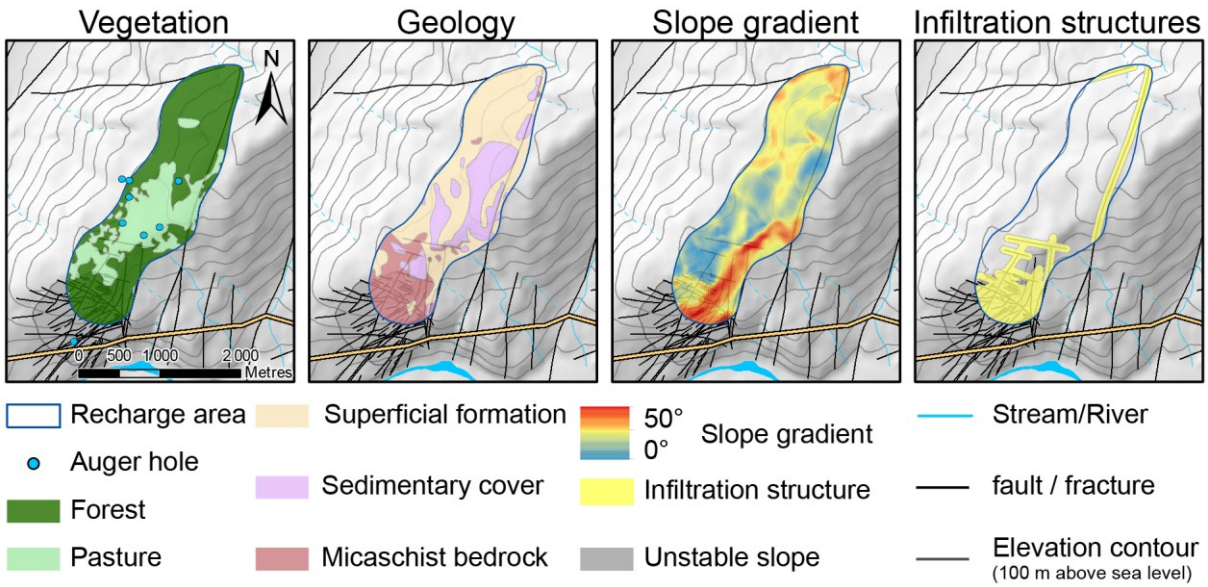

Fig. 6: Factor sub-areas, auger holes and infiltration structures used for the estimation of recharge-area parameters

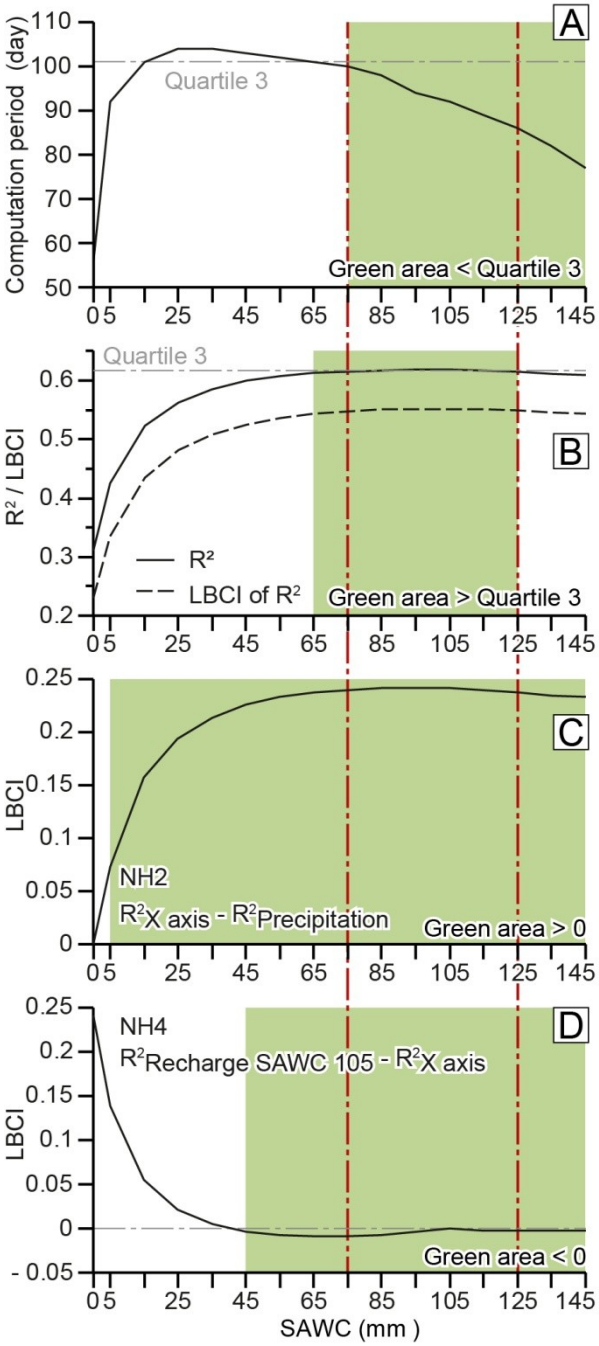

Fig. 7: Results of the sensitivity analysis relative to SAWC (soil-available water-capacity) for (A) the computation period, (B) the R^2 and the LBCI of R^2, (C) the LBCI of the null hypothesis NH2 and (D) the LBCI of the null hypothesis NH4. LBCI is the lower bound of the confidence interval

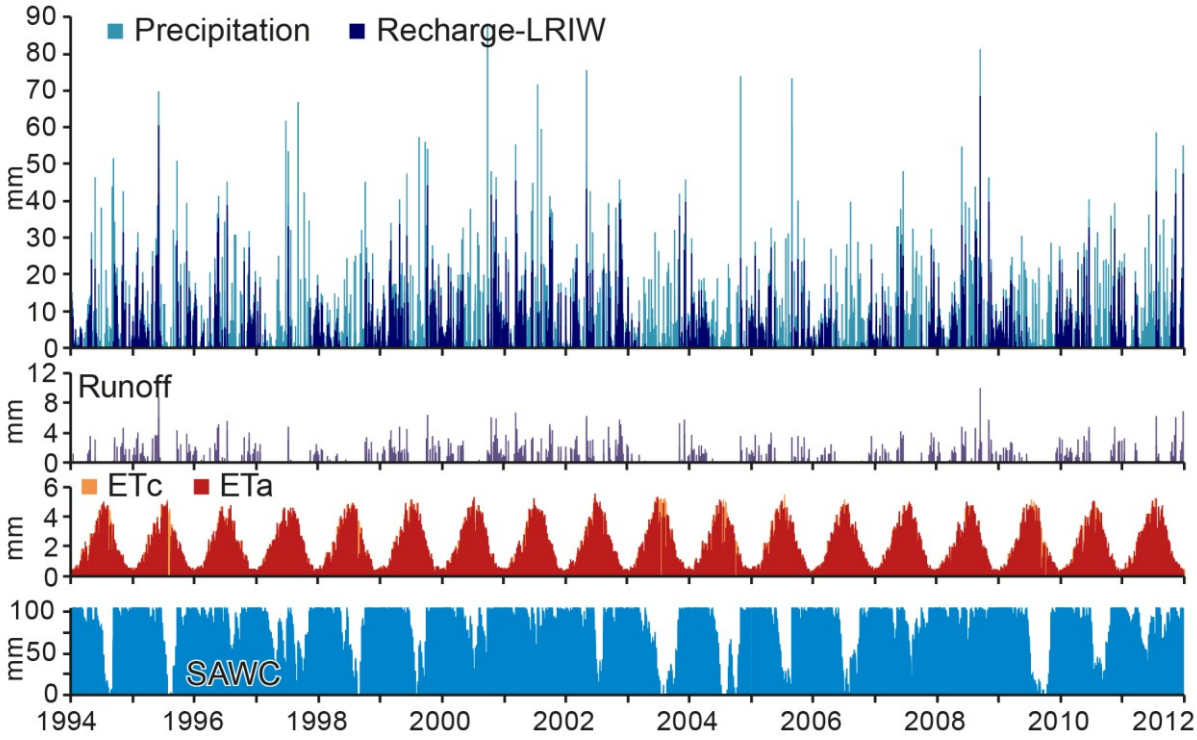

Fig. 8: Recharge computation with the LRIW method at Séchilienne with an SAWC of 105 mm and a runoff coefficient of 12.8%. ET_c: specific vegetation evapotranspiration; ET_a: actual vegetation evapotranspiration, SAWC: soil-available water-capacity

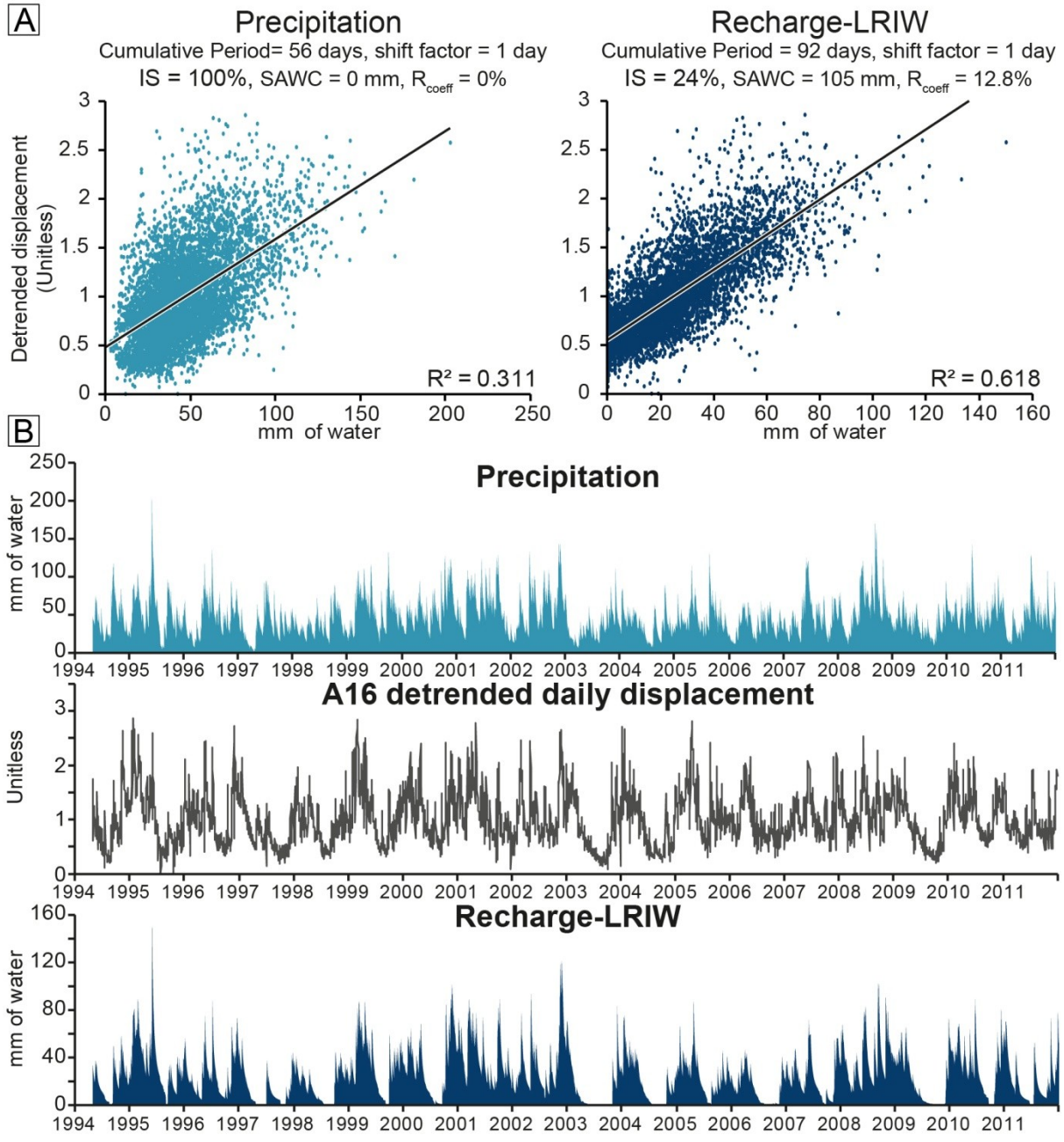

Fig. 9: Best linear correlation for precipitation and recharge computed with the LRIW method. IS is for infiltration structures. SAWC is soil-available water-capacity. Cumulative period (n) and shift factor (β) are the terms of the equation (3). A: Linear regression between precipitation/R_{LRIW} and A16 detrended displacement. B: Correlation between precipitation/R_{LRIW} and A16 detrended displacement as a function of time

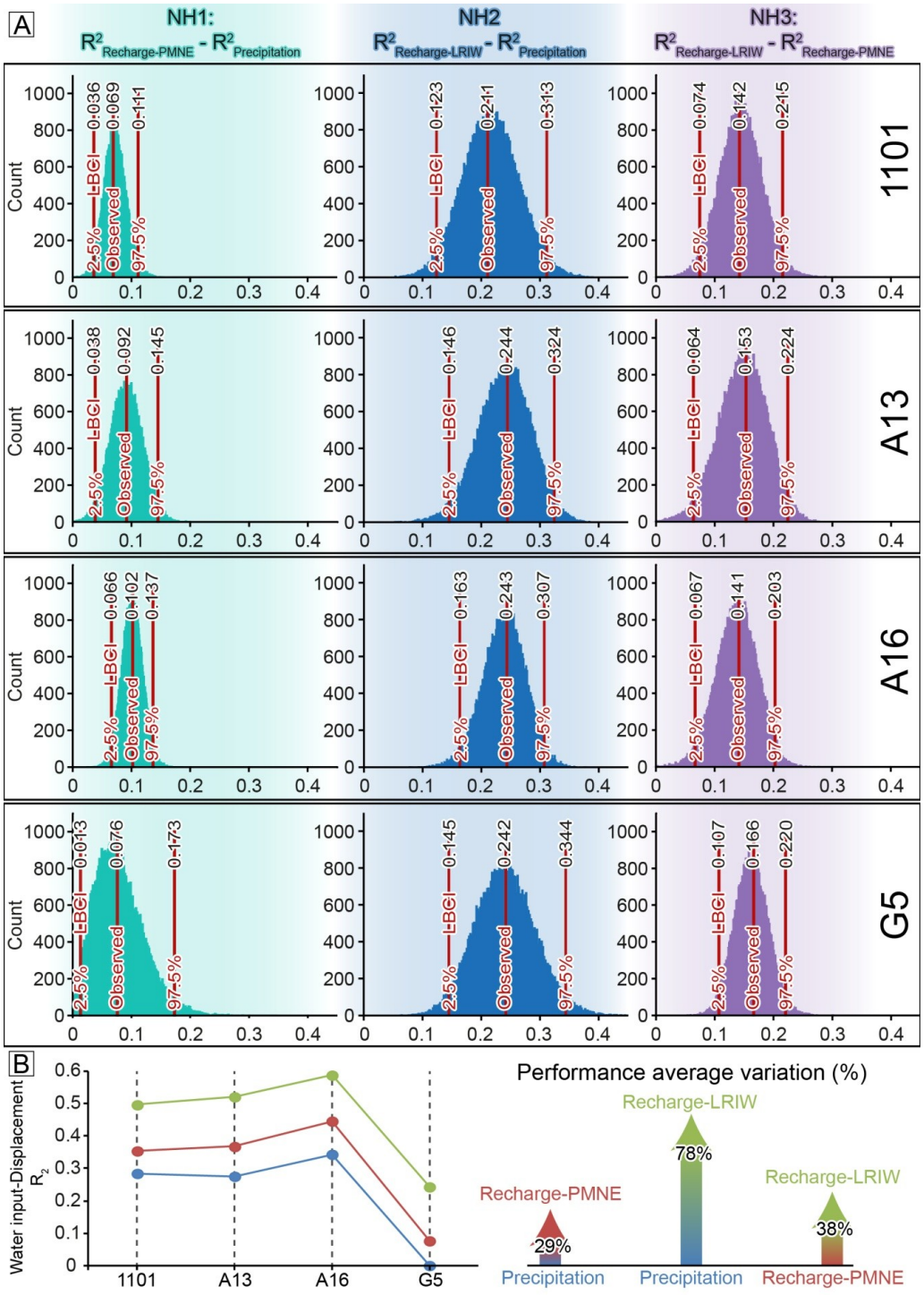

Fig. 10: Performance of the LRIW workflow. A: Bootstrap distribution of null hypothesis NH1, NH2 and NH3 tests for four displacement recording stations. LBCI is the lower bound of the confidence interval. B: R^2 values for the four displacement recording stations obtained with the precipitation, recharge-PMNE, and recharge-LRIW. LBCI is the lower bound of the confidence interval. G5 station is disregarded in the calculation of the performance average variation calculation since the R^2 value obtained at G5 from precipitation is close to 0, therefore leading to a non-representative variation.